J. Fluid Mech. (1989), *vol.* 198, *pp.* 27–64
Printed in Great Britain

Pattern-recognition analysis of the velocity field in plane turbulent wakes

By J. A. FERRÉ AND FRANCESC GIRALT
Departament d'Enginyeria Quimica i Bioquímica, Divisió VII, Universitat de Barcelona, 43005, Tarragona, Catalunya, Spain

(Received 2 October 1987 and in revised form 9 May 1988)

A pattern-recognition procedure designed to extract footprints of organized structures from turbulent signals is developed and used to analyse the large-eddy organization of several turbulent wake flows. The pattern-recognition technique is intended to be a general-purpose analytical tool that makes no use of specific flow characteristics, and that can be implemented as a computer code independent of the types of signals to be processed. The technique is applied to analyse the wake generated by a single cylinder at downstream positions ranging from $x/D = 10$ to $x/D = 220$. Also the structural features of the wakes behind a rotating cylinder, two cylinders of unequal diameters and two cylinders of equal diameter, one rotating, are examined at $x/D = 140$. In the near wake the large-scale motions detected are Kármán vortices, whose periodic activity persists up to 60 diameters. Further downstream the most significant coherent structures detected are single and double rollers with shear-aligned vorticity, whose dimensions and velocity intensities are properly scaled by the half-width of the wake and the local r.m.s. values, respectively. The similarities observed in the organized motions identified in the different wakes at $x/D = 140$, suggest that the roller organization may be an intrinsic characteristic of fully developed turbulent plane wake flows, irrespective of initial conditions.

1. Introduction

In recent years, a rather well-ordered picture of several turbulent flows has evolved among turbulence researchers (Cantwell 1981; Hussain 1983). One of the first fully developed turbulent flows found to contain large-scale ordered motions was the turbulent far wake (Townsend 1956; Grant 1958). However, most past studies on the analysis of the large-scale organization of turbulence have been carried out in boundary layers and mixing layers, probably owing to the great technological interest of the former flows and to the occurrence of well-ordered motions in the latter (Roshko 1976), which surprised many researchers (Laufer 1975). In addition, the techniques of conditional sampling (or phase averaging) and flow visualization, which were successfully applied to shear layers and boundary layers to reveal the organization of these flows, seem inadequate for the analysis of fully developed turbulent wakes and jets.

Another class of flow exhibiting a high degree of organization is the near wake flow behind bluff bodies. Apart from the early visualizations of the Kármán vortex shedding process (Prandtl & Tietjens 1934), the most useful information on the topology of the near wake flow has been obtained by conditional averaging or phase averaging techniques (Davies 1976; Cantwell & Coles 1983; Hayakawa & Hussain 1985; Kiya & Matsumura 1985).

From a comprehensive set of correlation measurements at $x/D = 533$, Grant (1958) postulated that large-scale motions in the far wake consisted of a double-roller organization, with vorticity roughly aligned with the axis of the mean rate of strain, and of 'mixing jets' that he envisaged as ejections of turbulent flow from the centre of the wake towards the irrotational external flow. Even though it has been pointed out that there is not a unique relation between the instantaneous velocity field and the correlation tensor (Cantwell 1981), the results obtained by Keffer (1965, 1967) in a wake strained through a constant-area distorting duct, gave support to Grant's hypothesis. In addition, the orthogonal decomposition technique developed by Lumley (1965), when applied by Payne & Lumley (1967) to the correlation data obtained by Grant (1958), again suggested a roller organization in the far wake. In this case, however, it has to be recognized that the large eddies depicted by Payne & Lumley were slightly tilted anti-shearwise at their centres, instead of along the shear axis as suggested originally by Grant.

Most of the visualizations of the far wake (Grant 1958; Taneda 1959; Keffer 1967; Papailiou & Lykoudis 1974) have presented side views of this flow. However, even in the case of a wake generated by an infinite cylinder without end effects, the turbulent flow downstream is essentially three-dimensional in the instantaneous velocity field. The statistical two-dimensionality observed in the mean velocities, turbulence intensities and higher moments is a consequence of the fact that there is not a preferred spanwise alignment, and averaging over a long period of time produces the same results independent of the vertical slice of the flow scanned. Also, when an 'instantaneous' photograph is taken, rather than the streamwise evolution of the wake, what is observed sometimes are slices through different spanwise positions of a three-dimensional organized motion of finite size, as may be seen for example in figure 11 of Cimbala (1985). Furthermore, additional caution has to be exercised when interpreting such photographs because of the differences between pathlines, streaklines and streamlines in a non-stationary flow (Kurosaka & Sundaram 1986) and because of the influence of the location where the marker is introduced and where the flow is observed (Cimbala 1985).

Barsoum, Karwall & Keffer (1978) reported measurements of the spanwise structure of a turbulent far wake. They observed that the bulges within the wake were 'quite narrow, and hence, being of limited lateral extent, strongly three-dimensional in nature'. This marked three-dimensional character of the flow, added to the impossibility of applying phase-averaging techniques to fully developed turbulent flows, has limited the knowledge of the large-scale organization of the turbulent wake to the original description of Grant (1958) and precluded obtaining further pictorial or anemometric evidence of roller organization in the far wake until very recently (Mumford 1983).

Townsend (1979) detected groups of spanwise vortices with vorticity aligned with the cylinder axis using a set of anemometers spatially distributed in the fully developed region of the wake. Savill (1979) modelled the effects of rotation and distortion on the wake flow using rapid distortion theory in conjunction with some hypothesis on the relative contribution to the turbulent activity of the fine-scale turbulence, the roller eddies and the Kármán-like vortices. Furthermore, based on the technique formerly used by Townsend (1979), he designed a pattern-matching technique for the detection and identification of large-scale motions, which was further developed by Mumford (1982), who analysed the roller structure in a turbulent plane jet (Mumford 1982) and in a turbulent wake (Mumford 1983). A more detailed account of the work of Townsend (1979), Savill (1979) and Mumford (1982,

1983) will be given concurrently with the analysis of the results presented in the following sections.

The present work has two main objectives. First, to develop within a pattern-recognition framework an organized-motion detector, based upon the work of Mumford (1982), in order to show the limitations and capabilities of such a technique when used as an analytical tool for the structural characterization of fully developed turbulent flows. And secondly, to analyse the structural similarities of the large-scale structures in a family of wakes generated by a single stationary or rotating cylinder, pairs of unequal diameter cylinders at rest and pairs of equal diameter cylinders, one stationary and one rotating, with the aim of establishing the dependence of the large-scale motions on the initial conditions. The flows analysed correspond to a wake with a Kármán vortex street (single cylinder), an asymmetric wake (unequal diameter cylinders), a distorted wake with inhibited vortex shedding (rotating cylinder) and a distorted and asymmetrical wake (one cylinder stationary and one rotating).

2. Experimental and analytical techniques for the analysis of organized motions in turbulent flows

The first fully turbulent flow that showed evidence of organized motion when examined by means of visualization was the turbulent boundary layer (Kline *et al.* 1967; Corino & Brodkey 1969; Kim, Kline & Reynolds 1971). However, much of the present interest on coherent structures in free shear flows arose from the well-ordered behaviour of the turbulent mixing layer, first observed by Brown & Roshko (1974). In both cases, as well as in other flows containing ordered motions, visualization was successfully used as a research tool to display the organized features of turbulence. However, it was difficult to obtain from correlation measurements clear evidence of the organization of these flows (Laufer 1975) and new analytical techniques were gradually developed to extract from the anemometric signals the information that conventional correlation measurements were not able to reveal.

One of the first conditional techniques applied to study boundary-layer flows was the quadrant decomposition of the Reynolds stress as a function of the sign of the fluctuating velocities (Wallace, Eckelmann & Brodkey 1972; Lu & Willmarth 1973). This procedure can be understood as a generalization of the concepts on conditional sampling introduced by Corrsin and Townsend in the 1950s for the analysis of intermittency. Interesting bibliographical surveys on conditional sampling were published by Van Atta (1974) and Antonia (1981). Later, conditional averages generated by two or more indicator functions were used by Keffer *et al.* (1982) and Andreopoulos (1985), among others.

A qualitative change in the experimental and analytical techniques used to study organized motions in turbulent flows occurred with the development of the VITA (Variable Interval Time Averaging) technique. This method was used by Blackwelder & Kaplan (1976) and by Chen & Blackwelder (1978) for the analysis of the velocity and temperature signals, respectively, in a turbulent boundary layer. The breakthrough attained with VITA was the success in separating random contributions from repetitive trends embedded in a signal by means of ensemble averaging (sometimes referred to as phase averaging owing to the kind of problems that were first treated this way, see for example Reynolds & Hussain 1972) using an indicator function sensitive to the occurrence of organized motions and which provided the phasing signal necessary for ensemble averaging. Other types of detector functions and special experimental arrangements based on conditional sampling

procedures have been developed since then to obtain ensemble averages of organized structures contained in different turbulent flows.

There are detection procedures that make use of some external triggering or phasing signal, and others that obtain the indicator function from the same signal that has to be averaged. One of the advantages of a technique based in an external reference signal is that spatial maps of the coherent structures can be obtained either using a conditional sampling procedure (Hussain 1983), or a conditional averaging technique in connection with a flying hot-wire arrangement (Perry & Watmuff 1981; Cantwell & Coles 1983). However, problems derived from phase jitter (Blackwelder 1977; Yule 1980) when the triggering and sampling points separate from each other, limit the applicability of the technique and, what is more restrictive, the success of a detection scheme depends on the selection of a relatively clear and skewed reference signal, and thus on the specific characteristics of the flow under study.

Conversely, one can recognize, within the analytical tools used for the study of boundary layers, techniques that build the phasing signal from the same quantities that have to be averaged. This is the same procedure used in the study of the intermittence and, in fact, the short-time variances used in the VITA scheme and some of the alternative techniques described by Subramanian *et al.* (1982) can be identified as indicator functions previously used in intermittence analysis. One of the general limitations of such techniques is that it is not possible to perform the detection and ensemble averaging on-line and, therefore, the spatial maps of the organized structures have to be changed in time-footprints or time-history of the structures while crossing the anemometers. Nevertheless, the kind of signals and experimental conditions that the boundary-layer techniques are capable of successfully handling are much more complex in terms of random components of the signal, random appearance of the burst, etc. than those able to be treated by conditional sampling procedures.

Unfortunately, the VITA technique is not of general use for the study of organized motions in turbulent flow because the detection procedure is based on local energetic criteria, a feature that may not be shared by all the different types of organized motion. In this sense, the pattern recognition approach of Wallace, Brodkey & Eckelmann (1977) avoids making implicit use of the high level of turbulent activity associated with the bursting phenomena. On the other hand, however, it is a fully syntactical pattern-recognition code that, while allowing detection of bursts in a wide range of scales, will hardly be easily applied to the analysis of signals with a high content of noise or with unknown characteristics.

A technique that can be of general use in extracting trends from very random signals is the method used by Zilbermann, Wygnansky & Kaplan (1977) to improve the ensemble averages obtained under significant misalignment. The procedure involved the cross-correlation of the raw signal with the current ensemble average, in order to determine the best alignment of the data windows that formed a new ensemble average in an iterative procedure where the zero iteration was obtained by a conditional sampling arrangement. In a study of the large eddies in a wake and in a boundary layer, Townsend (1979) also made use of local cross-correlation measurements to infer from anemometric signals the structural characteristics of the flow. What is much more important in his work, from the point of view of a detection procedure, is, first, that he assumed that if the large eddies were really 'large' their passage had to be simultaneously sensed by a set of anemometers widely spaced in the flow. Secondly, he tested the kind of large-scale trends registered by the

anemometers comparing an eddy model with the experimentally recorded signals by means of their instantaneous cross-correlation.

Further developments of Townsend's ideas were carried out by Savill (1979). Mumford (1982) described a 'pattern recognition and image enhancement' procedure that established the basis of the pattern-recognition technique presented in this paper and which uses a velocity model to check the structural characteristics of the flow. This procedure does not need the knowledge of the flow patterns beforehand and permits bounding the number of different patterns recognizable in a particular set of data. A further advantage of the procedure to be described is that it can be easily implemented as a computer code for the analysis of turbulent signals, independent of the flow under study and of the patterns that one hopes to identify. In the following sections a large-scale motion-detection scheme for turbulent flows based on previous pattern-recognition ideas will be introduced. Its characteristics, advantages and shortcomings will be analysed from a pattern-recognition point of view.

3. A pattern-recognition technique for the detection of large-scale motions in turbulent flows

The most difficult step in establishing the foundations of a large-scale eddy motion-detection scheme is to produce an appropriate definition of a large-scale ordered motion which is flow-feature independent. This is not an easy task as various authors seemed unable to adopt a common nomenclature, let alone common definitions. While Grant (1958) and Townsend (1976, 1979) referred to 'large eddies', Mumford (1982, 1983) used 'large eddies' and 'organized structures' as synonymous, and Cantwell in his review (Cantwell 1981) preferred 'organized motion'.

More recently, Hussain (1983, 1986) has proposed the 'coherent structures' description. Hussain (1983) defined a coherent structure as 'a connected, large scale turbulent fluid mass with a phase-correlated vorticity over its spatial content'. In accordance to this definition, Hayakawa & Hussain (1985) have used a large-scale detection technique based on the evaluation of the instantaneous large-scale vorticity field from velocity data sampled by a set of $\times$-wire anemometers. The coherent structures (in that case Kármán vortices in the wake of a circular cylinder at $x/D = 10$ to $x/D = 40$) were detected as closed contours of iso-vorticity and were aligned for ensemble averaging by picking up first the peak vorticity positions and by improving the average later with a procedure similar to that described by Zilbermann *et al.* (1977). This technique allowed the identification of the large-scale organization of the flow studied. However, the computation of the vorticity from the $\times$-wire signals requires an assumption about the convection velocity of the organized motion. Also interpolation is needed to obtain the vorticity at midpoints between anemometers, and the technique is limited to the use of sets of aligned $\times$-wires.

Our aim is to set up the basis of a general procedure to extract repetitive trends embedded in apparently random signals. Therefore we prefer to define a turbulent ordered motion in a wide sense as a flow organization, characterized by some typical velocity, vorticity, etc. distribution over a spatial region, which is frequently recurring, even though in most cases at random intervals, and is capable of yielding a statistically significant ensemble average. This definition has no direct link with vorticity dynamics, and can be considered excessively signal-processing oriented.

Nevertheless, we believe this to be a desired feature in our definition to distinguish the characteristics of the analytical tools used from the significance of the results that those can provide when they are interpreted from a turbulence dynamics point of view, in the same sense, for example, as spectral analysis may be used, irrespective of whether the flow under investigation exhibits any periodicity or coherence.

Three stages are involved in the present approach. The first is to adopt a 'minimum' definition for the ordered motion, that does not imply any specific connotation when considered in the turbulent context. This connotation is, in fact, what is intended to be evaluated, and cannot be assumed in advance. The second stage is that, owing to the random character of the turbulent signals, any assessment of organization cannot be supported on the basis of individual realizations but has to be significant in the sense that there exist a subset of realizations that can be averaged to obtain a representative mean, which, in turn, is significantly different from the conventional one. The 'significant difference' can be objectively evaluated using a statistical significance test to ascertain the probability of obtaining such different values by chance. And the third stage is that once some ordered, non-random motion is definitely observed in a set of data, the results have to be scrutinized from the fluid mechanical point of view to see if they shed new light on the turbulence dynamics.

To state the procedure in more physical terms, let us assume that the flow under investigation is being observed from an Eulerian frame of reference. Suppose that by means of some non-intrusive technique yet to be developed, it were possible to repeatedly sample instantaneously and simultaneously, at a set of densely packed points spanning some fixed volume, a momentum-balance related quantity (velocity, vorticity, ...) or the concentration of some suitably introduced marker (heat, for example), and that an unconditional ensemble-averaging procedure were carried out to obtain mean values of the measured variable at each point. If one suspected that the turbulent flow contained some kind of organization, it would be possible to obtain an ensemble average using only selected sets of points (simultaneously sampled over the sampling region) from the population that contributed to the conventional average. The conditional ensemble average obtained in this way would, in general, be different from the conventional one, and the probability that the differences occurred only by chance would have to be tested for statistical significance. If finally it could be demonstrated that the ensemble averages were significantly different, one would be able to conclude that an organized motion had been detected. However, a statistically significant result does not automatically imply a result of practical importance, unless the difference between observed means is of the same order of magnitude as the means themselves, and the organized motion detected can be demonstrated to play some important role in that turbulent flow.

In this hypothetical experiment, one can observe an important feature. If no rotation or scaling is allowed, not all the topologically similar flow organizations will be recognized as belonging to a family of organized structures. From the point of view of rotation it is necessary to point out that if the organized motion appears with a random orientation the problem is suitable for statistical treatment. In fact, some of the early ideas of organized eddies in turbulent flows attempted to describe isotropic turbulence as a random superposition of a family of deterministic vortices. A discussion of these models can be found in Saffmann (1981). Moreover, from the point of view of the scale or size, it has to be taken into account that larger flow organizations are less likely to have random orientations, because they are more sensitive to the boundary conditions of the flow (in free shear flows they are

effectively confined by the turbulent/non-turbulent interface), while smaller ones are candidates for more random orientation. These are some of the reasons why, although the possibility of occurrence of organized motion is not necessarily confined to the large scales, evidence of ordered motion has been observed mainly in the large scales of turbulent flows.

In the following, attention will be concentrated upon the large-scale motion of turbulent wakes. By definition, a large-scale organized motion spreads its influence over a large region of the flow. Therefore it should be possible to study such large-scale motions by means of the analysis of the footprints they leave over a set of sensors widely spaced within the flow, the spacing between sensors being of the order of some characteristic lengthscale of the bulk flow (i.e. the half width of the wake) and the overall span of the sensors being of the order of the total width of the shear flow.

Probe interference effects and economic constraints usually oblige the substitution of the spatial downstream coordinate of the volume scanned by a temporal coordinate. Then, instead of spatial distribution, we have to analyse time histories of the structures while crossing the anemometers. This implicitly necessitates the use of Taylor's hypothesis of frozen turbulence, in assuming that the structures do not change significantly during the time interval in which they are sensed, although it is not necessary to explicitly transform the time coordinate into spatial displacements. The number of sampling points (anemometers, thermometers, etc.) that have to be used, and their relative position (alignment, geometrical distributions...) are a matter of preference (or possibly necessity). A set of anemometers aligned with either the y-axis (shear coordinate) or the z-axis (spanwise coordinate) sampling 'slices' of the flow, seems to be one of the most reasonable arrangements because the two-dimensional array of sampled velocities in (y, t) or (z, t) coordinates can be processed to extract information of the organized motion with vorticity aligned along the z-axis (spanwise structures with circulation in an (x, y)-plane) or the y-axis ('three-dimensional' structures with circulation in an (x, z)-plane).

Suppose that a turbulent variable, $\boldsymbol{D}$, has been simultaneously sampled at $i = 1, 2, \ldots i_x$ points (not necessarily equally spaced or aligned), thus obtaining a two-dimensional array of data that can be written as $D(i,j)$, $i = 1, 2, \ldots, i_x$, $j = 1, 2, \ldots, j_x$. The detection scheme to be designed has to be able to select all the data frames or windows of size (k_x, l_x) points containing the same kind of time patterns in order to obtain their ensemble average

$$\langle D(i,j)\rangle = \langle D\rangle(k,l) = \lim_{m_x \to \infty} \frac{1}{m_x} \sum_{m=1}^{m_x} D[I(m)+k, J(m)+l]$$

$$(k = 1, 2, \ldots, k_x; \quad l = 1, 2, \ldots, l_x) \quad (1)$$

where $I(m)$ and $J(m)$ are vectors containing the starting points of all the data frames to be averaged. Without lack of generality, let us assume that $k_x = i_x$ to simplify the following discussion. Later it will be shown that the technique easily expands to unequal sizes. If j_0 is the beginning of an arbitrary data frame $H(k, l)$ of size (i_x, l_x), then

$$H(k,l) = D(i,j) \quad (k = 1, 2, \ldots, i_x; \quad l = 1, 2, \ldots, l_x);$$

$$(i = 1, 2, \ldots, i_x; \quad j = j_0+1, j_0+2, \ldots, j_0+l_x). \quad (2)$$

Any data frame corresponds to a point in a c_x-dimensional vector space, $P(c)$, $c = 1, 2, \ldots, c_x$, with $c_x = i_x l_x$, through the relation

$$P(c) = P(k+(l-1)\,i_x) = H(k,l) \quad (c = 1,2,\ldots,c_x;$$

$$k = 1,2,\ldots,i_x; \quad l = 1,2,\ldots,l_x), \quad (3)$$

and all the data frames that can be taken from the data, for $j_0 = 0, 1, \ldots, (j_x - l_x)$, form an ordered set of vectors spanning the pattern space.

The pattern-recognition problem is how to establish a partition of the pattern space in such a way that all the points in one partition belong to the same family or class of those predefined by some rule or feature. Sometimes the features that distinguish one class from another are unknown and the approach is to recognize the clouds that arise from the natural grouping of points.

The different cases commonly encountered in a two-dimensional space are those depicted in figure 1. Figure 1 (*a*) shows the case where the points are not naturally grouped and it is difficult to define a general criteria on how to partition the pattern space in different classes. Figure 1 (*b*) depicts a situation with three different classes and the partitioning can be established simply by selecting the lines that limit the regions containing each family (linear discriminant analysis). Alternatively, the classification can be performed if the natural clouds that appear are recognized and single or multicentred 'clusters' of neighbouring points are formed (clustering analysis). In a multidimensional space the points cannot be visualized so easily and special techniques have to be applied (Bow 1984). Finally, figure 1 (*c*) presents a case that could only be handled by minimum-spanning tree or similar techniques.

It is worth investigating in more detail the idea of 'natural' classification underlying the clustering algorithms regardless of the suspicion that the plot of the vector patterns arising from turbulent signals is going to be more similar to the grouping of figure 1 (*a*) than that of figure 1 (*b*). To be able to evaluate closeness between points, a measure of distance has to be introduced, and if the coordinates in the pattern space have been appropriately normalized or have the same weight in defining different features, the use of an Euclidean distance δ between two points, $\boldsymbol{P}$ and $\boldsymbol{Q}$, is the obvious choice,

$$\delta^2(\boldsymbol{P},\boldsymbol{Q}) = \frac{\Sigma\,[P(c)-Q(c)]^2}{\Sigma Q(c)^2}, \quad (4)$$

where the modulus of the vector $Q(c)$ has been chosen as a normalizing factor. Let us evaluate the quality of such measure of closeness or similitude in a problem arising from a turbulent flow. A large-scale motion detector is expected to exhibit at least three properties:

(i) Not perturbed or distorted by the background, fine-scale turbulence. If possible, we would like to design a detector fully independent of the noisy effects of the fine-scale turbulence over a wide range of signal-to-noise ratios.

(ii) Amplitude independent, i.e. prepared to detect and classify correctly large-scale motions even in the case where their energy content is low. This can be reformulated saying that the same decision has to be taken for two footprints differing only by a multiplicative factor.

(iii) Size independent.

The size independent feature is by far the most difficult to fulfil. If the detection scheme is not based on a fully syntactic rule, independent of the spatial and temporal coordinates – as is the case of the pattern-recognition scheme proposed by Wallace

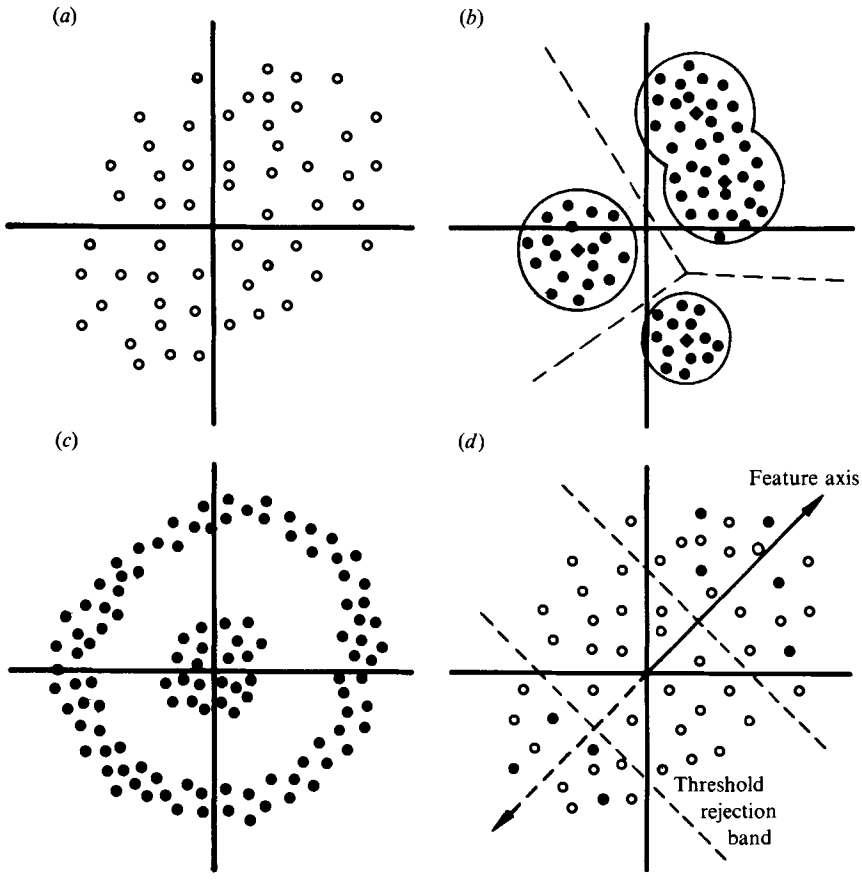

FIGURE 1. Examples of grouping in the pattern space. (*a*) No apparent grouping. (*b*) Families of points that can be classified by linear discriminant analysis or clustering. (*c*) Families of points not separable by clustering. (*d*) Classification of points in the pattern space selecting feature axis by means of correlation measurements.

et al. (1977) – but is built upon the hypothesis that organized motions will be recognized by the simultaneous effects produced in a set of sensors, then the selection of a particular probe spacing implies the selection of a limited range of sizes. Only in the case of a very dense grid of sampling points could one expect to detect organized motions within a range of sizes from one to ten.

In the case of the pattern-recognition analysis carried out by Wallace *et al.* (1977) in a boundary layer, only one sampling point was used at a high sampling rate. The coordinate representative of the footprint to be detected was known in such detail that a series of patterns and sub-patterns could be selected. Otherwise, if we recall the definition of coherent structure as a large-scale organized motion spanning the full width of the flow, it appears that as the coherent structure size decreases, the importance of such organization as large scale also decreases. Even though size-invariant pattern-recognition schemes have been developed in the past (Altmann & Reitbrok 1984; Lahart 1984), it has to be pointed out that the real limitation of the size-independent condition is the maximum number of anemometers that could be used in an experiment.

The success of a pattern recognition scheme in handling noisy signals is related to

the common idea of filtering. Obviously a low-pass filter can remove the high-frequency fluctuations, producing a smooth signal. However, filtering *per se* is questionable in at least three aspects. First, it remains unanswered where the patterns are located in the filtered version of the signals, because even in the case of filtering a quantity such as vorticity that could be directly used as a large-scale detector, the filter action consists of smoothing the signal and not in defining a detection criteria. Secondly, not all the high-frequency components of a signal are due to fine-scale turbulence. The Fourier transform of a box-shaped function, for example, spans from the lowest frequencies to the highest values through successive ripples of decreasing amplitude but containing an important amount of energy. One can argue that the coherent organization of any flow is not going to be box-shaped, but the same reasoning applies to footprints containing sharp gradients. And thirdly, the specifications of a filter are set in the frequency domain and any relation to the time domain, i.e. to the spatial coordinates, is, therefore, lost.

Nevertheless, the smoothing properties of filters are extremely important. Consider the case where the Euclidean distance is accepted as the criteria to evaluate if a specific pattern belongs to the class represented by a prototype $Q(c)$. Suppose, in addition, that the pattern $P(c)$ to be classified is exactly the prototype buried in noise of zero mean, i.e. $P(c) = Q(c) + N(c)$ with $\Sigma N(c) = 0$. If the normalizing factor is chosen to be the length of the prototype, the distance between $P(c)$ and $Q(c)$ is given by

$$\delta^2(\boldsymbol{P}, \boldsymbol{Q}) = \frac{\Sigma [P(c) - Q(c)]^2}{\Sigma Q(c)^2} = \frac{\Sigma N(c)^2}{\Sigma Q(c)^2} > 0. \tag{5}$$

It can be deduced that not only is the pattern to be recognized contaminated by noise but also the decision that is going to be taken. If the signal-to-noise ratio is very high, the threshold value in the acceptance criteria can be relaxed, but as the noise becomes more and more important the probability of wrong decisions increases quickly. It is easy to check that the amplitude independent condition is not accomplished because

$$\delta^2(s\boldsymbol{Q}, \boldsymbol{Q}) = (1-s)^2, \tag{6}$$

where s is a scaling factor. We are going to show why such a measure of similitude is noise dependent. If the numerator of (5) is expanded,

$$\Sigma [P(c) - Q(c)]^2 = \Sigma P(c)^2 + \Sigma Q(c)^2 - 2\Sigma P(c)\, Q(c), \tag{7}$$

and each individual term is expressed as a function of $Q(c)$ and $N(c)$ only, and the uncorrelation between $Q(c)$ and $N(c)$ is used to reduce all summations $\Sigma Q(c) N(c) = 0$, it follows that

$$\Sigma P(c)^2 = \Sigma [Q(c) + N(c)]^2 = \Sigma Q(c)^2 + \Sigma N(c)^2, \tag{8a}$$

$$\Sigma Q(c)^2 = \Sigma Q(c)^2, \tag{8b}$$

$$\Sigma P(c) Q(c) = \Sigma Q(c)^2. \tag{8c}$$

It is clear that the noise dependence is produced by the term $\Sigma P(c)^2$, i.e. the modulus of the vector $P(c)$. However, the cross-correlation term does not contribute to the final value, but simply cancels out with the other terms. This suggests that if instead of the Euclidean distance the cross-correlation between the prototype and the pattern to be classified was introduced as a measure of similitude or 'closeness' in the pattern space,

$$r(\boldsymbol{P}, \boldsymbol{Q}) = \frac{\Sigma P(c)\, Q(c)}{\Sigma Q(c)^2}, \tag{9}$$

then noise independence could be reached. It is easy to show that a vector including uncorrelated noise gives the same correlation coefficient as a 'clean' one

$$r(\boldsymbol{Q}+\boldsymbol{N},\boldsymbol{Q}) = r(\boldsymbol{Q},\boldsymbol{Q}) = 1. \tag{10}$$

The amplitude-independent condition is not exactly fulfilled. This deviation is of minor importance, as will be shown later, because the value of the correlation obtained is not equal to unity, but exactly the amplitude factor

$$r(s\boldsymbol{Q},\boldsymbol{Q}) = s. \tag{11}$$

When the cross-correlation coefficient is expressed as a function of the test pattern $T(k,l)$, $k = 1,2,\ldots,i_x$, $l = 1,2,\ldots,l_x$ and of the recorded data $D(i,j)$, $i = 1,2,\ldots,i_x$, $j = 1,2,\ldots,j_x$, it can be written as a two-dimensional array $R(m,n)$, $m = 1$, $n = 1,2,\ldots,(j_x - l_x + 1)$ with only one row

$$R(m,n) = \frac{\dfrac{1}{i_x l_x}\sum_{p=1}^{i_x}\sum_{q=1}^{l_x} D(p,q+n-1)\,T(p,q)}{\left[\left(\dfrac{1}{i_x l_x}\sum_{i=1}^{i_x}\sum_{j=1}^{j_x} D(i,j)^2\right)\left(\dfrac{1}{k_x l_x}\sum_{k=1}^{k_x}\sum_{l=1}^{l_x} T(k,l)^2\right)\right]^{\frac{1}{2}}} \tag{12}$$

where the normalizing factor has been chosen to be the product of the mean r.m.s. values of $T(k,l)$ and $D(i,j)$. The two-dimensional form is introduced to extend the procedure to the case of different width of data and test pattern matrices that will be presented later.

As a consequence of the fact that the different patterns or data frames which have to be classified are obtained in an ordered manner, consecutive data frames with increasing values of the cross-correlation coefficient indicate that alignment between the test pattern and the window of data is improving, until a local maximum in the cross-correlation function is obtained, i.e. until the best concordance or similitude between the test pattern and the recorded turbulent signal is attained. Thus, the decision of accepting or rejecting a data frame as belonging to the class represented by some prototype, depends only upon the values of the local extrema of the correlation function being higher or lower, respectively, than a pre-selected threshold value. This value has to be low enough to allow patterns equal to the prototype but with intensity reduced by a scaling factor to be classified correctly. In fact it is only necessary to discard the very low maximum values of the correlation function to obtain threshold-invariant ensemble averages.

The smoothing properties of the correlation operation arise from the fact that cross-correlating is equivalent to convolving, and convolution is the time domain expression of a filtering process. The main differences with respect to a standard filtering operation are that the filter applied in this case is designed not from the frequency domain specifications, but from the time domain, and that filtered signals are taken as an indicator of the time-lag necessary to reach the best alignment in the ensemble average. This procedure is similar to that used by the 'matched filtering' techniques of signal identification (Whalen 1971). The latter has the disadvantage, however, that the (matched) filter is designed to detect a known signal buried in noise and the filter specifications have to be known exactly. This is not the case of the problem under study because one wants to design a detection scheme not only able to extract known characteristics but powerful enough to discover unknown or even unexpected features. Let us split the problem into two subproblems; how to obtain

an initial estimate of the large-scale footprints? And second, having obtained an initial estimate how to improve it?

The improvement of initial estimates can be achieved from the ideas of clustering analysis. If an initial estimate is obtained for each of the patterns to be detected, the pattern space can be partitioned into a known number of classes (as many classes as different initial patterns selected) by classifying each point as belonging to the class represented by the 'more similar' prototype (the initial estimate). Once the pattern space is partitioned, new cluster centres can be evaluated as the mean value of all points belonging to one class and the process can be iteratively repreated until no significant displacement of the cluster centre is observed (Bow 1984). This procedure, stated in terms of data frames and ensemble averages, implies that once one ensemble average is obtained it is used as the starting point for a new iteration, a procedure that continues until no significant variation in the features displayed by the ensemble average is detected. This iterative procedure first described by Mumford (1982), ensures that even in the case of a bad initial estimate, the genuine features of the data being processed can be extracted.

How to obtain an initial estimate of the large-scale footprints and how many 'different' footprints can be detected, are two questions with very different answers. From a pattern-recognition point of view it can be deduced how many different patterns one can expect to distinguish in a given experimental situation. However, the form of the initial estimates have to be inferred from the previous knowledge (and sometimes prejudices) of the flow under study. Savill (1979) and Mumford (1982, 1983) choose their initial patterns from the analysis of correlation data. Often one can handle this problem by establishing a full set of 'possible' patterns and running the pattern-recognition algorithm for each one of them. From the results obtained by Ferré & Giralt (1989) in a thermally contaminated wake it is evident that even such a black-box approach gives very good results.

In a pattern space like that presented in figure 1 (*b*) there can be identified as many different classes as non-overlapping closed lines can be drawn, i.e. as many as points in the pattern space. However, it has to be remembered that the condition of noise independence implies the substitution of a conventional distance measurement by a cross-correlation coefficient, which corresponds to the inner product of the two vectors $P(c)$ and $Q(c)$. Since $Q(c)$ is a fixed vector and $P(c)$ is only one term in the series of consecutive data frames formed from the data, the classification procedure can be understood as the selection of the vectors that locally have the highest projection over the direction determined by the vector $Q(c)$. The partition of the pattern space by means of the correlation measurements and the iterative procedure based upon the ensemble averaged patterns, are not procedures for selecting independent clouds of points, like those in figure 1 (*b*), but for obtaining successive approaches to the principal feature axis of the pattern space†. This situation is depicted in figure 1 (*d*), which illustrates the equivalence of the cross-correlation procedure and the computation of projections for each vector over the feature axis. Only local extrema in the correlation function and only a small number of selected points from the pattern space are subjected to a decision procedure and are classified

† From equations (5), (8) and (9) it can be observed that the substitution of an Euclidean distance by a correlation measure implies losing the information brought by the modulus of the vector $P(c)$. While this leads to the desired noise-independence condition, the triangle rule is broken, i.e. if $Q1$, $Q2$ and $Q3$ define a triangle then $\delta(Q1, Q2) + \delta(Q2, Q3) \geqslant \delta(Q1, Q3)$. This inequality does not hold for r measures instead of δ. This is the reason why the procedure is not able to form, strictly speaking, 'clusters', but only to select 'feature axis'.

as members of one class or rejected by the threshold band. This band not only rejects the weakest patterns, but also contains the vectors mainly aligned with the axis perpendicular to the current feature axis.

From linear algebra, we know that any set of c_x linearly independent vectors can be used as a basis for a c_x-dimensional space, although a set of orthogonal vectors is preferable. This means that c_x linearly independent patterns can be distinguished within the data if the windows used in the pattern recognition are of size $c_x = i_x l_x$. For example, a common experimental arrangement with a set of eight anemometers sampling u-velocities at 5 kHz per channel in a turbulent flow, with large-scale motions extending over time lengths of the order of 20 ms, would lead to an 800-dimensional space. The problem is not as untreatable as it may seem at first glance, because the pattern space is 800-dimensional, but the feature space is, at least, one order of magnitude smaller.

The problem is then how to pre-process the data in order to reduce the dimensionality of the pattern space to that of the feature space. It has to be taken into account that the limited number of sensors used imposes in the spatial direction a sampling period usually one or two orders of magnitude below the A/D sampling rate. Thus, the individual values of data obtained in the high-density sampled coordinate have to be appropriately grouped or concentrated in a single point to produce an equally spaced array of samples in both dimensions. If such 'feature extraction' stage is used before the pattern-recognition analysis is carried out, the problem becomes choosing among a small number of different patterns. In fact, it is not necessary to reduce the dimension in a pre-processing stage, because cross-correlating the data with the test pattern does it automatically. However, this reduction is useful as a conceptual tool to understand how many 'different' patterns can be detected in a given set of data.

The best basis for a vector space is that formed by orthogonal vectors because they fulfil the condition of linear independence as a whole and are, one by one, independent. From the point of view of the pattern space, the orthogonality is a desirable property because, observing orthogonal (independent or uncorrelated) ensemble averages, we are sure that the features depicted by each individual ensemble average are not contaminated or mixed with those depicted by a second one. Consequently, if a simultaneous classification of the pattern space is planned, the different initial test patterns have to be selected uncorrelated. Sometimes, however, the pattern recognition analysis can be developed using single classification criteria in consecutive stages. Once one feature axis is extracted, i.e. an invariant ensemble average is obtained from some initial estimate, the same data can be processed with an initial test pattern independent of the former ensemble average, and so on. Both techniques have been used in the present work and will be discussed in conjunction with the analysis of the different wake flows studied.

Although not explicitly stated, it has been assumed up to now that the raw data being processed were of some turbulent scalar variable (u-velocity, temperature). The technique can be easily expanded to handle velocity signals obtained by an array of $\times$-wire anemometers or even by an array of multiple-wire probes, distributed in a two- or three-dimensional space. The only change that would have to be introduced in these multidimensional cases is in the cross-product between the test pattern and the raw data given by equation (12). If the point by point product between scalars can be expressed as the inner product between vectors, all the procedures described can be adapted to process vectorial data. Obviously, in this case, the test pattern has to be also a matrix of vector velocities and the ensemble average has to consist of

averaging vectors instead of scalars. This could be a different approach to the technique presented by Hayakawa & Hussain (1985), because the vorticity content of a particular data frame would also be checked, not directly over the instantaneous vorticity map but by comparison to the vorticity content of the test pattern.

4. Experimental equipment and data acquisition

All the wake flows analysed were generated in an open-circuit, suction-type wind tunnel, with flow continuously controlled in the range 1–20 m/s by a variable speed fan. The test section was 600×600 mm^2 by 3 m long. A set of flow straighteners and filters, in combination with a 9:1 contraction zone produced a flow with a free-stream turbulence less than 0.4%.

Figure 2 shows the different cylinder configurations used and their sizes. All data were obtained at a Reynolds number based on the free-stream velocity and the cylinder diameter of 9000. When more than one cylinder generated the wake flow, the Reynolds number was referred to the largest diameter. This resulted in free-stream velocities of about 7 and 11.3 m/s for cylinder diameters of 19.3 and 12 mm, respectively.

Eight normal-wire constant-temperature anemometers (DISA 55M01/55M10 bridges and 55P11 probes), operated at an overheat ratio of 1.8, were used to sample the turbulent u-velocity signals in the wakes. The anemometers were calibrated assuming a King's law relation,

$$\frac{E^2}{(R_w - R_g)} = A + BU_{ef}^n, \tag{13}$$

where E is the bridge voltage, R_w and R_g the operating and cold wire resistances, respectively, U_{ef} the effective cooling velocity and A, B and n constants obtained by calibration. The anemometers were calibrated in the empty test section of the wind tunnel, with velocities measured with a Pitot tube connected to a differential-pressure cell, and anemometer voltages obtained via A/D conversion.

The data acquisition was carried out with a 12-bit A/D converter DIGITAL ADFO1, supported by a PDP 11/60 computer. The A/D converter had a 16-channel single-ended multiplexed input, with a maximum sampling rate of 400 kHz, provided with alternate-buffer capabilities. The effective maximum sampling rate for continuous data acquisition was limited by the maximum writing speed of the disk pack. A complete set of data acquisition and file handling programs were written to allow physical input/output, thus increasing the effective maximum sampling rate from 16 kb/s (unformatted WRITE from FORTRAN) to 160 kb/s, i.e. 80 kHz because 12 bits were stored in a word of two bytes.

The voltage signals were centred to zero by subtracting the d.c. component, amplified, low-pass filtered at 2 kHz and sampled at 5 kHz per channel. The low-pass filters were second-order IIR Butterworth filters. For each set of experimental conditions the data acquisition system was calibrated to reduce inaccuracies. In all experiments, continuous records of 40 s were digitized, copied onto magnetic tapes and processed in an IBM 3083 computer at CIUB (Informatic Centre of the University of Barcelona).

Data acquisition in the family of wakes described was performed in two perpendicular planes as shown in figure 3. The spacing between anemometers was selected to be 0.6 l_0 (l_0 is the half width of the wake as defined in figure 3), thus covering the whole velocity defect zone in the vertical plane and an equivalent region

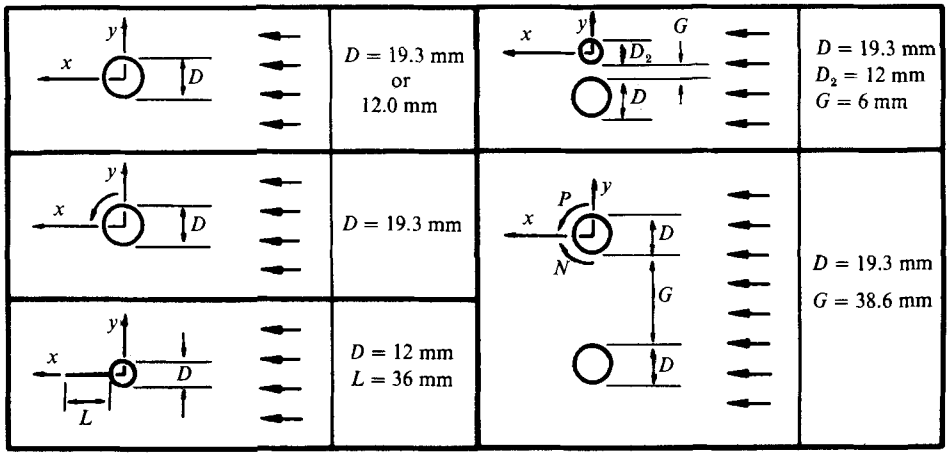

FIGURE 2. Wake configurations.

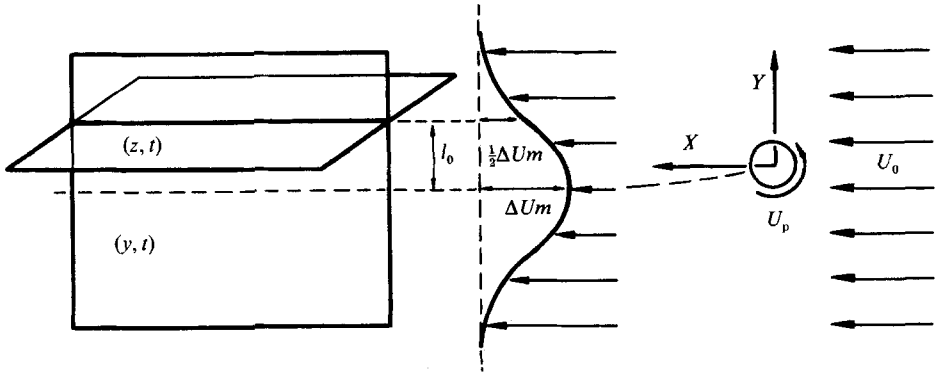

FIGURE 3. Flow configuration and sampling planes.

in the horizontal one. Table 1 includes the information about all relevant parameters related to the anemometer arrangements. It should be noted that in the near-wake experiments the spacing between anemometers was altered, as depicted in table 1. When the wakes under study were symmetric, data were recorded only in one horizontal plane, but when the wakes were asymmetric both upper-half and lower-half horizontal planes were separately investigated. In those cases the set of anemometers was centred in the dynamical field of the wake rather than in the geometrical centre (see figure 3).

5. The pattern-recognition algorithms

Two pattern-recognition computer codes were developed to analyse the recorded turbulent signals. As the sampling points used in each case were equally spaced and aligned, a further extension of the principles established in the preceding sections can be developed. If the number of sampling stations available were enough to cover a region an order of magnitude greater than the width of the wake, the selection of patterns of organized motion, in both horizontal and vertical planes, would reduce to the identification of sub-frames within the matrix of data points. However, the sampling stations barely cover the width of the flow and while in the vertical plane

Wake	x/D	Plane	l_0/D	Spacing/l_0	U_p/U_0
S	10	$(y,t)^a$	0.90	0.45	—
S	30	(y,t)	1.45	0.9	—
S	60	(y,t)	2.17	0.6	—
S	60	(z,t)	2.17	0.6	—
S	100	(z,t)	2.82	0.6	—
S	140	(z,t)	3.31	0.6	—
S	140	(y,t)	3.31	0.6	—
S	220	(z,t)	4.05	0.6	—
R	140	(y,t)	2.30	0.6	1.5
R	140	$(z,t)^b$	2.30	0.6	1.5
R	140	(y,t)	1.83	0.6	2.0
R	140	$(z,t)^b$	1.83	0.6	2.0
SP	140	(y,t)	2.83	0.6	—
SP	140	(z,t)	2.83	0.6	—
DU	140	(y,t)	3.90	0.6	—
DU	140	$(z,t)^b$	3.90	0.6	—
DR	140	(y,t)	4.0	0.6	0.0
DR	140	(z,t)	4.0	0.6	0.0
DR	140	(y,t)	3.0	0.6	−2.0
DR	140	$(z,t)^b$	3.0	0.6	−2.0
DR	140	(y,t)	3.0	0.6	2.0
DR	140	$(z,t)^b$	3.0	0.6	2.0

S, single cylinder; R, rotating cylinder; SP, cylinder with trailing splitter plate; DU, two unequal cylinders; DR, two cylinders with one of them rotating.

[a] Anemometers spanning over the half upper wake.

[b] Data available for both upper and lower side of the wake.

TABLE 1. Sampling stations and experimental conditions.

one can expect to locate organized motions within the bounds of the irrotational flow, in the horizontal ones the effect would be very different.

If there is no preferred spanwise alignment, the set of anemometers will be sensing only a portion of the structures or perhaps misaligned structures. As a consequence and following the work of Mumford (1982) a test pattern wider than the data matrix was used to ensure the detection of any kind of organized motion, irrespective of their spanwise alignment. This situation is illustrated in figure 4, where a test pattern spanning the width of 12 hypothetical anemometers is shown aligned over a data matrix of only 8 anemometers. In terms of the correlation function over which the detection procedure has been based, this new situation leads to a two-dimensional correlation function $R(m,n)$, $m = 1,2,\ldots,(k_x - i_x + 1)$, $n = 1,2,\ldots (j_x - l_x + 1)$,

$$R(m,n) = \frac{\dfrac{1}{i_x l_x} \sum_{p=1}^{i_x} \sum_{q=1}^{l_x} D(p,q+n-1)\,T(p-m+k_x-i_x+1,q)}{\left[\left(\dfrac{1}{i_x l_x}\right) \sum_{i=1}^{i_x} \sum_{j=1}^{j_x} D(i,j)^2 \left(\dfrac{1}{k_x l_x} \sum_{k=1}^{k_x} \sum_{l=1}^{l_x} T(k,1)^2\right)\right]^{\frac{1}{2}}}. \tag{14}$$

The organized motions are detected again as local extrema over a two-dimensional domain. In other words, for each value of $n = 1,2,\ldots,n_x$ the best transversal alignment is selected in $m = 1,2,\ldots,m_x$, and among the best transversal alignments

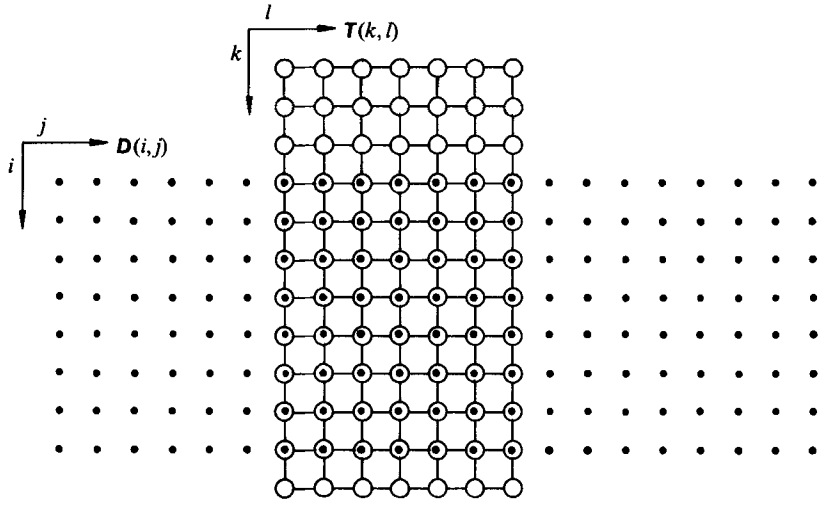

FIGURE 4. Data matrix and test pattern.

local extrema along the longitudinal coordinates are identified as pointers of the frames of data containing some specific organization.

5.1. *Generation of test patterns*

The test pattern used as starting points in the clustering algorithms have been generated simulating the passage of known vortices across a set of anemometers while convected by a turbulence-free mean flow. It should be noted that with u-velocity data only it is more difficult to establish a relation between the flow patterns observed and the stream function or iso-vorticity contours of the rollers. In what follows, some examples of synthetic experiments with 'anemometers' sensing stream function, vorticity and u-velocity are presented first. The family of vortices used in the simulated experiments is described by a stream function Gaussianly damped (Townsend 1976)

$$\psi(x,y,z) = \psi_0 f\left(\frac{x}{x_0},\frac{y}{y_0},\frac{z}{z_0}\right)\exp\left\{-\frac{1}{2}\left[\left(\frac{x}{x_0}\right)^2+\left(\frac{y}{y_0}\right)^2+\left(\frac{z}{z_0}\right)^2\right]\right\} \tag{15}$$

where ψ_o, x_0, y_0 and z_0 are arbitrary normalizing and size parameters. The velocity field induced by the vortex is

$$U = -\partial\psi/\partial y, \quad V = \partial\psi/\partial x, \quad W = 0. \tag{16a,b,c}$$

If the vortex axis is free to be randomly oriented with respect to the anemometer reference axis, a whole family of instantaneous velocity patterns can be generated. The function $f(x/x_0, y/y_0, z/z_0)$ controls the zeros of the stream function and vorticity of the modelled vortex. For example, if $f = 1$, $x_0 = y_0$, and $z_0 \to \infty$, a two-dimensional infinite vortex with a bell-shaped stream function cross-section is obtained. This is the single-roller velocity-pattern model shown in figure 5. If $f = x/x_0$, a nodal plane for ψ is introduced and two side-by-side counter-rotating vortices that correspond to the double-roller model are obtained.

Figure 5 presents cross-sections or slices of the single- and double-roller vortices in terms of stream function, vorticity and u-velocity. These plots, as well as those generated by the pattern-recognition computer codes, are presented as iso-level

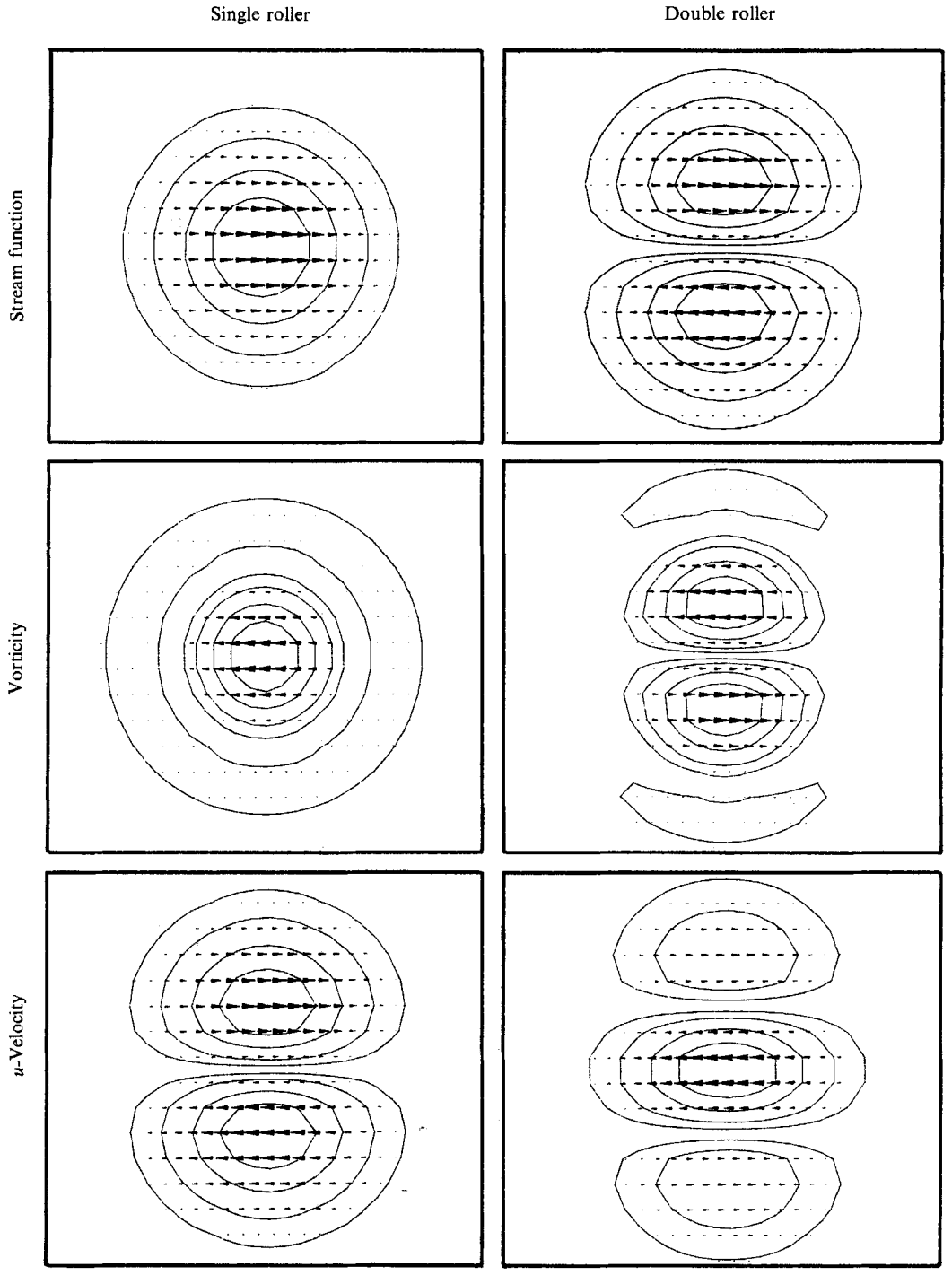

FIGURE 5. Cross-sections of the single- and double-roller vortex models.

contours at $\pm 10\%$, $\pm 25\%$, $\pm 50\%$ and $\pm 75\%$ of the peak signal. In addition, arrowheads have been added to show the sign and magnitude of the sampled quantity. The rule adopted has been the following: the horizontal axis is the time coordinate increasing from left to right and the vertical axis is the spatial coordinate z or y. Arrowheads are scaled to show relative magnitude and are directed to the left for negative values and to the right for positive ones. Both axes are always equally scaled so that the pattern presented are in 'natural' proportions (time coordinate units are converted in space coordinate units using a convective velocity equal to the mean velocity of the anemometer set). Since the probe gap is $0.6\,l_0$, all the ensemble averages presented will be $(N-1)\,0.6\,l_0$ high and $2(N-1)\,0.6\,l_0$ long in size. N is the number of anemometers of the ensemble-averaging window, and is equal to 12 in the analysis of the (z,t) data.

The above mentioned rule has a drawback which cannot be easily solved. As time increases, the time plots can be interpreted using Taylor's hypothesis as maps of the instantaneous spatial flow organizations that will cross the anemometers while convected by the mean flow from right to left, the anemometers being placed at the time origin along the vertical axis. This is the reason why flow sketches have been presented flowing to the left. However, positive velocity fluctuations, i.e. excess velocity over the time mean, are associated with arrowheads directed to the right, which is in accordance with the sign rule but inconsistent with the leftwards direction of the flow. As there is no way to make consistent the time and sign fluctuation axis, results will be presented as described. Thus, arrowheads have to be understood as giving correctly the fluctuation sign but showing inverted direction with respect to a right to left flow when representing u-velocities.

In figure 5 one can observe that single rollers will appear in the u-velocity maps as two lobes of u-velocity fluctuations, sign inverted. Furthermore, double-roller organizations will appear as a central lobe of negative flucatuations, flanked by weaker positive u-velocity contours. The effects of the lack of orthogonality between the vorticity axis of the vortex and the slicing plane, are the same as those produced by modification of the scaling parameters of the vortex (x_0 and y_0, in the plots presented). Then no information on the exact orientation of the vortex axis will be available because there is no way to distinguish between orientation effects and size effects.

Fabris (1979) simultaneously sampled u, v, w and temperature in the wake of a heated cylinder, using a special purpose multiwire probe. Figure 6 includes a few milliseconds of the data given in figure 11 of Fabris' paper, together with the simulated velocity and temperature signals. The vortex used is a two-dimensional one [$x_0 = y_0 \ll z_0$; $f(x/x_0, y/y_0, z/z_0) = 1$] with the circulation axis on a (x,z)-plane, but not parallel to the z-axis, in such a way that the W component of the velocity, as measured by the anemometer, is not zero. The temperature signal has been simulated using stream-function values and assuming that the surrounding flow is cold and only the vortex is hot. As can be observed in figure 6 the experimental and simulated values agree very well.

5.2. *Simultaneous double classification procedure*

Mumford (1983) described the problem of the misclassification produced by the lack of orthogonality between double and single rollers when transverse alignment is allowed. This problem is illustrated in figure 7. Though single and double rollers are uncorrelated when correctly aligned (figure 7*a*) the separate search of single and double rollers can produce in a data frame a maximum in the correlation function for

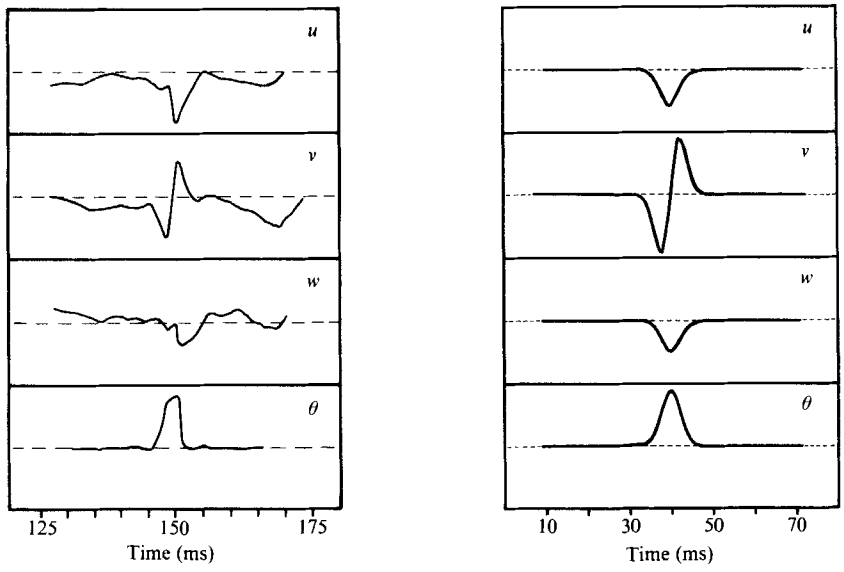

FIGURE 6. Comparison of the multiple-wire data of Fabris (1979) with the velocity and temperature footprints of a single roller.

the same longitudinal position, coordinate $n = 1, 2, \ldots, n_x$, but for different transverse alignments, coordinate $m = 1, 2, \ldots, m_x$ (figure 7*b*). This is the reason why, in addition to a single-classification algorithm, a double-classification code was used to analyse the roller organization in the horizontal plane.

The general layout of the algorithms is presented in figure 8. After cross-correlating the data D with each of the prototypes P1 and P2, individual frames are classified as belonging to some of the families C1 and C2 investigated or are rejected to the null class C0. The ensemble averages M1 and M2 are used iteratively as new prototypes until final patterns E1 and E2 are obtained. The classification is accomplished by accepting only the extrema (maximum or minimum) that appear centred in the transverse position within the correlation matrix of one class and is simultaneously bounded by two local extrema (maximum and minimum) in the correlation matrix of the second class. This procedure ensures that the pattern is classified appropriately because not only is it selected correctly by itself, but the lack of orthogonality is recognized and misalignment is avoided.

Figure 9 illustrates how the classification routine separates single from double rollers. The top and bottom indicator outputs show, in each case, the position for best transverse alignment each time that maximum or minimum values of the correlation function plotted in the central part are found. Patterns are detected when a centred maximum is accompanied in the second correlation matrix by extrema placed in the edges of the detection matrix. For example, at time 200 ms a maximum is observed for the single-roller correlation, bounded by two extrema in the double-roller correlation matrix, thus the pattern is classified as a single roller. It has to be pointed out that these refinements of the classification method are needed because of the reduced number of sampling points available and to the fact that if one pattern is composed of three elementary closed contours in its iso-level plots, frames with only two of those but better aligned than their surrounding patterns can be misclassified if only information coming from one test pattern is available.

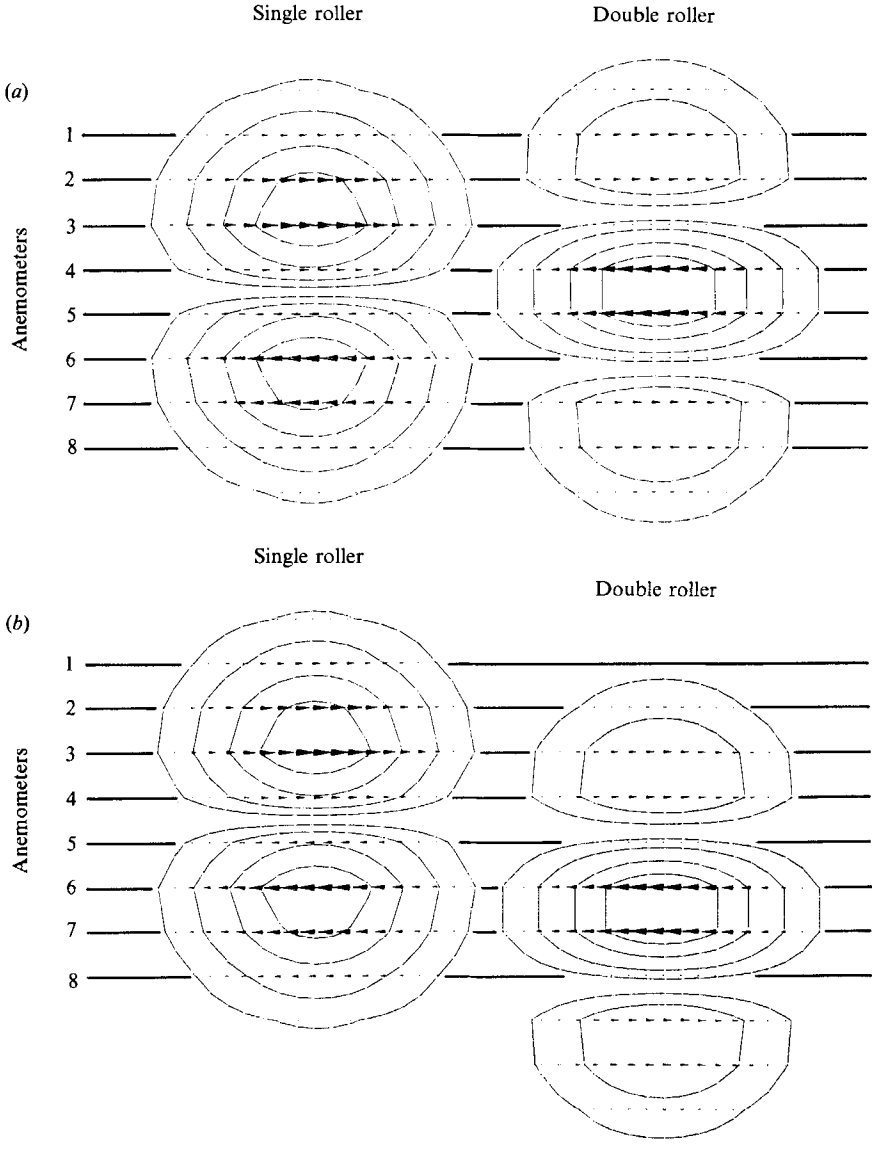

FIGURE 7. Single- and double-roller eddies misclassification. (*a*) uncorrelated single and double rollers. (*b*) correlated single and double rollers by transverse alignment.

A final comment has to be made on the pattern selection procedure. The cross-correlation procedure distinguishes between positive and negative patterns. While a distance-classifier would reject a data frame equal to the test pattern but sign-inverted, because in the pattern space both points are far away, $\delta^2(\boldsymbol{P}, -\boldsymbol{P}) = 4\Sigma P(c)^2$, the correlation-classifier recognizes this situation as a minimum in the correlation. Depending on the signals processed, both types of data frames can contribute to the same ensemble average after being sign-corrected. This is the case of the single-roller organization because for individual rollers both senses of rotation are equivalent. Sometimes only positive correlated frames are significant, and then negative extrema have to be discarded.

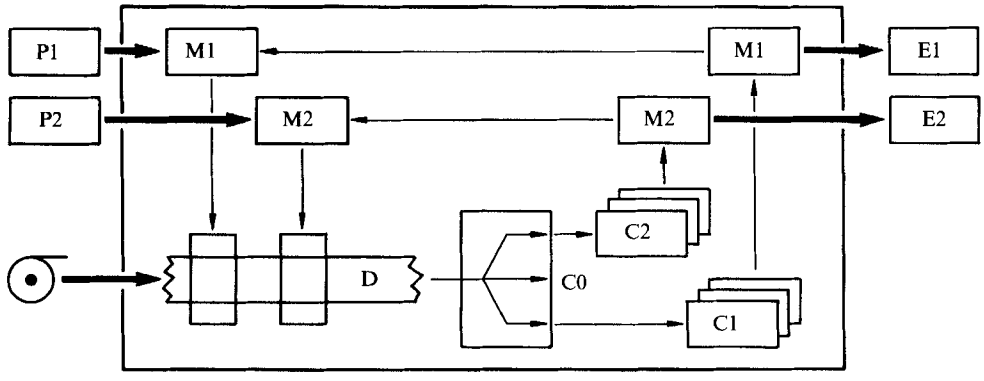

FIGURE 8. General layout of the pattern recognition algorithms.

Data normalization

The data sampled in the horizontal plane are obtained by a set of anemometers spanning along the homogeneous coordinate of the flow. Thus, it is expected that the statistics of the signals sampled by the different anemometers should be the same. This set of data is normalized by subtracting from the recorded velocities their time mean value and dividing by their individual r.m.s. If $D(i,j)$ is the matrix of velocities measured at locations and times (i,j) then

$$\overline{D(i)} = \frac{1}{j_x} \sum_{j=1}^{j_x} D(i,j) \quad (i = 1, 2, \ldots, i_x), \tag{17}$$

$$[D_{\text{r.m.s.}}(i)]^2 = \frac{1}{j_x} \sum_{j=1}^{j_x} [D(i,j) - \overline{D(i)}]^2 \quad (i = 1, 2, \ldots, i_x). \tag{18}$$

Thus, the normalized velocity matrix is given by

$$D_n(i,j) = \frac{D(i,j) - \overline{D(i)}}{D_{\text{r.m.s.}(i)}} \quad (i = 1, 2, \ldots, i_x; \quad j = 1, 2, \ldots, j_x). \tag{19}$$

Data corresponding to the vertical plane are normalized in the same way, with the r.m.s. value being the pooled estimate of data recorded at all locations. This pooled estimate is introduced to avoid overweighing the data from the anemometers located at the edges of the wake. From a computational point of view, things are simpler if the correlations are computed between sets of data with zero mean. However, the subtraction of individual mean velocities implies that the organized motions are detected as fluctuations deviating from the time-mean profile.

6. Statistical significance of structures

Most of the ensemble averages of coherent structures or large eddies reported in the literature have been obtained after their existence in the flow was revealed by visualization. In such cases the identity and reality of the detected structures were established without the support of any kind of significance test. In the present study, however, objective indicators of the statistical significance are applied to the ensemble averages to assess their significance level. Also, the fraction of the flow used

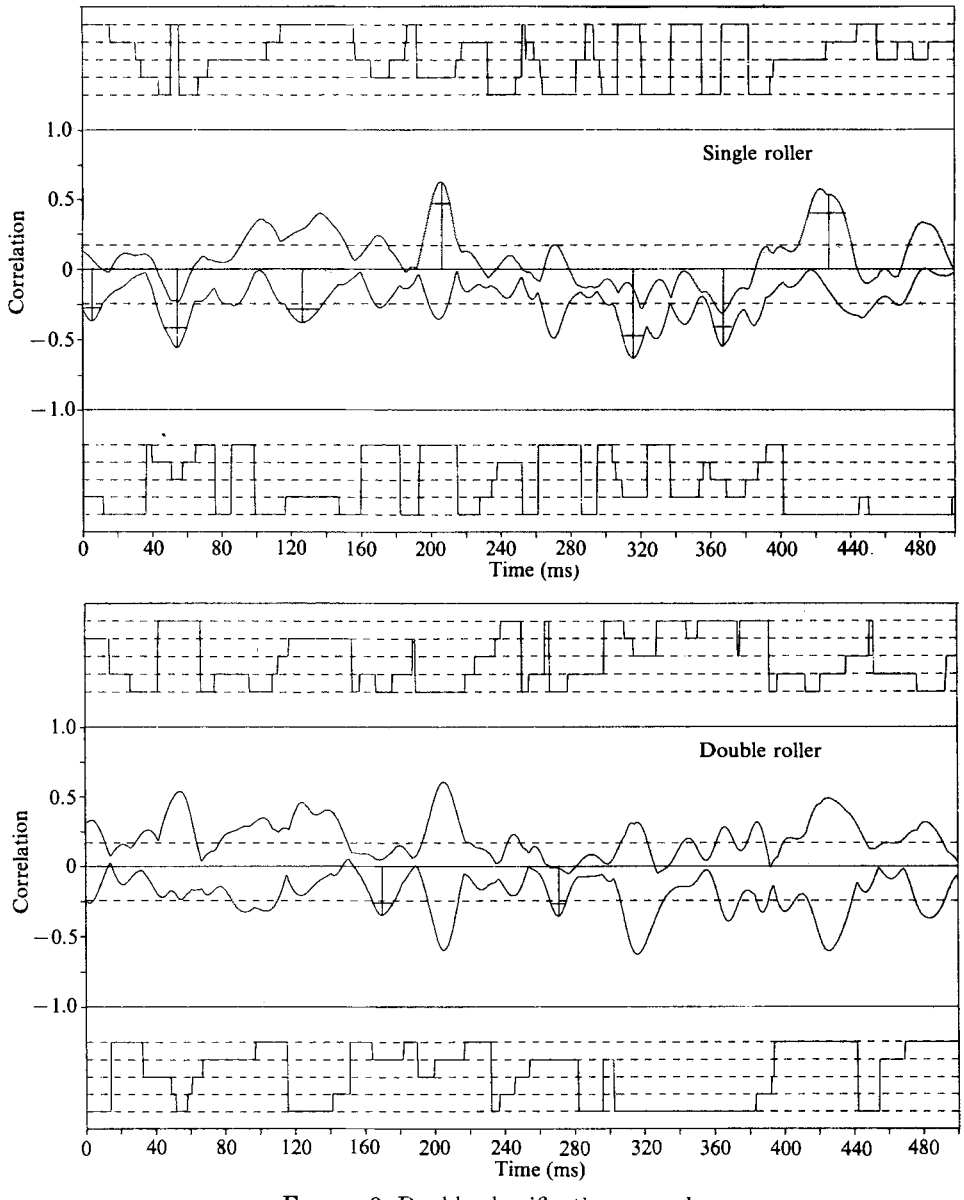

FIGURE 9. Double classification procedure.

to obtain each ensemble average is computed as an indicator of how important the structure in the flow is.

The statistical significance of the results obtained can be established by the level of significance of the plotted iso-contours ($\pm 10\%$, $\pm 25\%$, $\pm 50\%$, $\pm 75\%$ of the peak signal). The procedure described is only approximate because in the vertical plane the contours plotted enclose data from anemometers of different r.m.s. values, and in both horizontal and vertical planes not all the anemometers presented in the ensemble average are obtained by averaging the same number of patterns. The mean M of n points randomly selected from a population of zero mean and unit standard

deviation, has a p.d.f. that approaches a normal distribution with zero mean and standard deviation $1/n^{\frac{1}{2}}$, irrespectively of the form of the parent distribution, as n increases. As a consequence, the statistic,

$$Z = \frac{M}{1/n^{\frac{1}{2}}}, \tag{20}$$

can be considered to be a standard normal variable when $n > 30$. If a non-zero value of M is tested for the null hypothesis $H_0: M = 0$, the statistical significance of M being non-zero is given by the significance a of a two-sided test that puts M just in the critical value,

$$a = 1 - \frac{1}{(2\pi)^{\frac{1}{2}}} \int_{-Mn^{\frac{1}{2}}}^{Mn^{\frac{1}{2}}} \exp(-\tfrac{1}{2}Z^2)\,\mathrm{d}Z. \tag{21}$$

If the peak velocity or temperature were 1.0 r.m.s. units and the number of patterns averaged were 400, the $\pm 10\%$ contour would be significant at the level

$$a = 1 - \frac{1}{(2\pi)^{\frac{1}{2}}} \int_{-0.1\sqrt{400}}^{0.1\sqrt{400}} \exp(-\tfrac{1}{2}Z^2)\,\mathrm{d}Z, \tag{22}$$

that is, 5%. This means that the probability of obtaining a value for the lowest iso-level contour as high as 0.1 by chance is as low as 5% and, thus, the results could be considered significantly different from zero. The use of a $\pm 25\%$ contour will multiply the integration limits by a factor of 2.5 and the level of significance would be less than 0.01%. Since the signals handled by the pattern-recognition programs are always centred to zero, significant results are easily recognized as non-zero values in the ensemble averages.

The level of significance depends on the peak signal and on the number of patterns detected. For a given peak signal the level of significance is maximum when 100% of the flow is classified, i.e. when the number of patterns detected is only limited by the overlap condition and represents the whole set of data points. A greater level of significance could also be achieved recording more data. This is the reason why both the fraction of flow represented by one ensemble average and the level of significance have to be used to assess the significance and importance of the organized motions detected.

7. The roller organization in fully turbulent plane wakes

To analyse the structural characteristics of a plane wake, multiple-point data acquisition was performed behind a single cylinder at $x/D = 60$, 100, 140 and 220. Measurements were also carried out in the wakes of a cylinder with trailing splitter plate, a rotating cylinder and in the wakes generated behind a pair of unequal diameter cylinders and of a rotating and a stationary cylinder at $x/D = 140$. Details of these configurations are shown in figure 2 and table 1.

All the results and analysis that are presented in this section correspond to data obtained in the (z, t)-plane (see figure 3), i.e. with the set of anemometers aligned with the z-axis, at coordinates $y = l_0$ or $-l_0$ and $z = (0.6i - 2.7)l_0$, $i = 1, 2, \ldots, 8$. Thus, a plane view of the wake, instead of the usual side view, has to be retained in mind. In this geometrical set-up the anemometers will be sensitive to the large-scale organized motions with their vorticity aligned with an axis crossing the (x, z)-plane. The scales smaller than $0.6\,l_0$ will fall below the sampling grid while those larger than $4.2\,l_0$

would be indistinguishable from other kinds of organized motion producing same-sign velocity fluctuations in the set of anemometers.

Mumford (1983) showed that the typical large-scale organization of the fully turbulent plane wake was a three-dimensional roller motion that could be detected in the (z, t)-plane as double or single rollers. Based on these results, our analysis has been directed to the detection of the same kind of large-scale organization and, consequently, the data has not been checked for other types of structures. Figure 10 shows the analysis of the roller organization in the single-cylinder wake, from $x/D = 60$ to $x/D = 220$, while figures 11 (*a*) and 11 (*b*) are the single and double rollers used as initial test patterns. The analysis has been performed using the double classification algorithm. Data frames are classified as belonging to each of the classes represented by the test patterns, and both positive- and negative-correlated data windows are averaged. All results presented in figure 10 have normalized peak velocity values in the range 1.1–1.4 and, in each case, they represent approximately 45% of the recorded flow. The levels of significance of the 10% contour are over 5% (the worst value is 14%) for all stations, except at $x/D = 220$ where the significance is 4% and 1.8% for the single and double rollers, respectively. However, the 25% contours are always significant at levels lower than 0.1%, and the ensemble averages presented in figure 10 have to be compared taking into account the low significance of the regions contained between the 10% and 25% contours.

From the results included in figure 10 one can conclude that the present roller organization is coincident with the previous findings of Savill (1979) and Mumford (1983). Also, it can be inferred from our results that the roller organization remains substantially unchanged as the mean flow reaches self-similarity. It has to be noted that the differences observed in the rollers at $x/D = 220$ with respect to those at $x/D = 60$, 100 and 140 could be produced by the fact that data at $x/D = 220$ was obtained with the 12 mm diameter cylinder and higher potential flow speed, in order to maintain the same Reynolds number. As the sampling rate and the length of data recorded was not changed, this resulted in recording and analysing more flow. This is also the reason why the significance level is under 5% only at $x/D = 220$.

It is worth noting that the only scaling parameters that have been used are the half width of the wake and the r.m.s. values (mean velocity values are subtracted from velocity, but not multiplied). While the mean velocity profile could be collapsed in a self-similar curve beyond $x/D = 60$, this is not the case for the r.m.s. values. However one can conclude that the size of the rollers scales with the mean velocity parameters, while their intensity is more or less constant when scaled with the current r.m.s. value (a better scaling parameter would be the turbulent kinetic energy). Though more than 45% of the data have been classified in each analysis, no periodicities have been detected. The probability density function of the spacing between consecutive rollers shows occasional peaks, but broadly spread from low frequencies (say 10 Hz) to the highest values allowed by the non-overlap condition. Some grouping of rollers without any repetitive trend can be observed in figure 12, where a time distribution of events detected at $x/D = 220$ is presented.

Some selected results obtained in the wake of the rotating cylinder and of the cylinder with a trailing splitter plate at $x/D = 140$ are presented in figure 13. Both wakes correspond to initial conditions that modify the Kármán vortex shedding process. The trailing splitter plate used (see figure 2 for dimensions) retards the vortex shedding, which occurs at a lower Strouhal frequency, and causes the shedding of larger vortices (Apelt & West 1975). The rotation of the cylinder

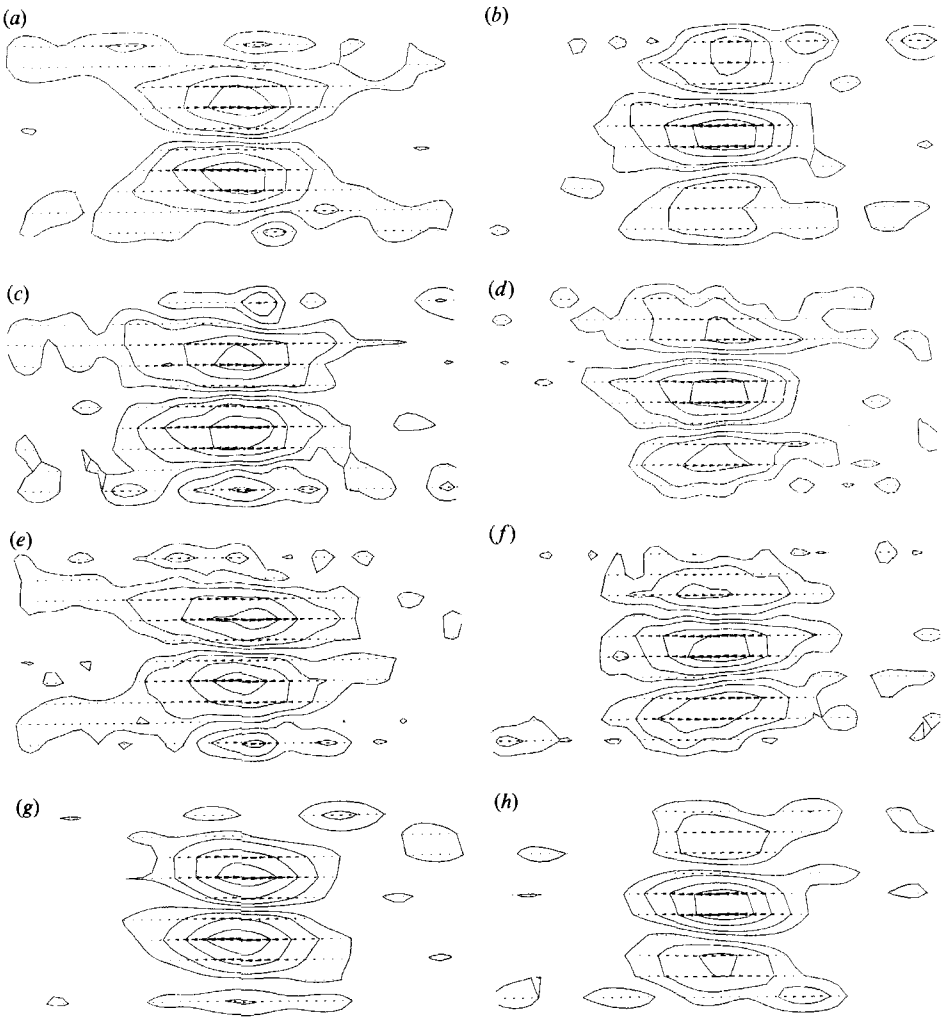

FIGURE 10. Single and double rollers in the wake of a cylinder. (a), (b) $x/D = 60$. (c), (d) $x/D = 100$. (e), (f) $x/D = 140$. (g), (h) $x/D = 220$.

progressively inhibits the Kármán vortex shedding as peripheral velocity increases. For $U_p/U_0 > 1.5$ no periodic activity is detected (Gavaldà 1982) while the flow is increasingly distorted.

The roller ensemble averages shown in figure 13 for the trailing splitter plate cylinder are very neat owing to the large number of structures recorded and analysed because in this case the 12 mm cylinder was also used. In this wake, peak velocity values are 1.15 and 1.35, for the single and double rollers, respectively. The significance level is under 2%, and the fraction of flow averaged is 49%. In the wake of the rotating cylinder, although the rollers detected are topologically coincident with those previously observed for other wakes, their size has decreased and their peak velocities are higher. The observed peak values are 1.65 and 2.01, for single and double rollers in the upper half wake, respectively, and 1.16 and 1.25 for the same structures in the lower part. Note that the initial distortion of the wake is propagated downstream and that at $x/D = 140$ the r.m.s. values are still 0.068 and 0.094 m/s in

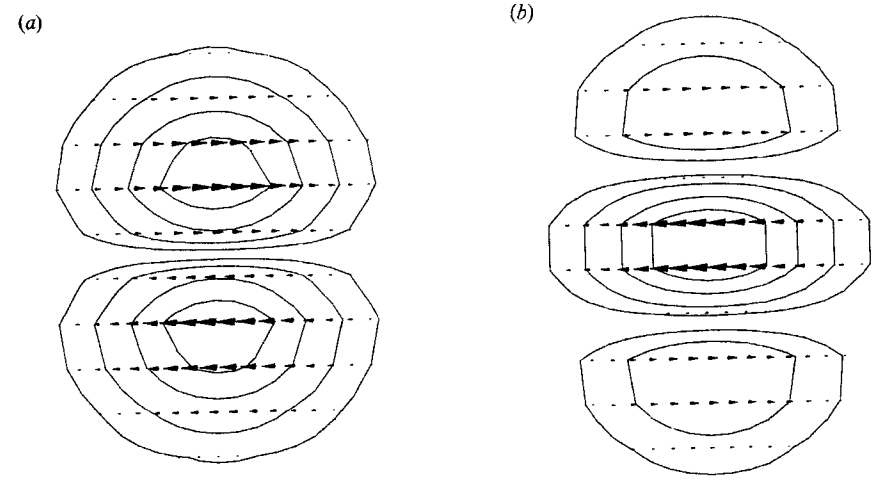

FIGURE 11. Test patterns. (*a*) Single roller. (*b*) Double roller.

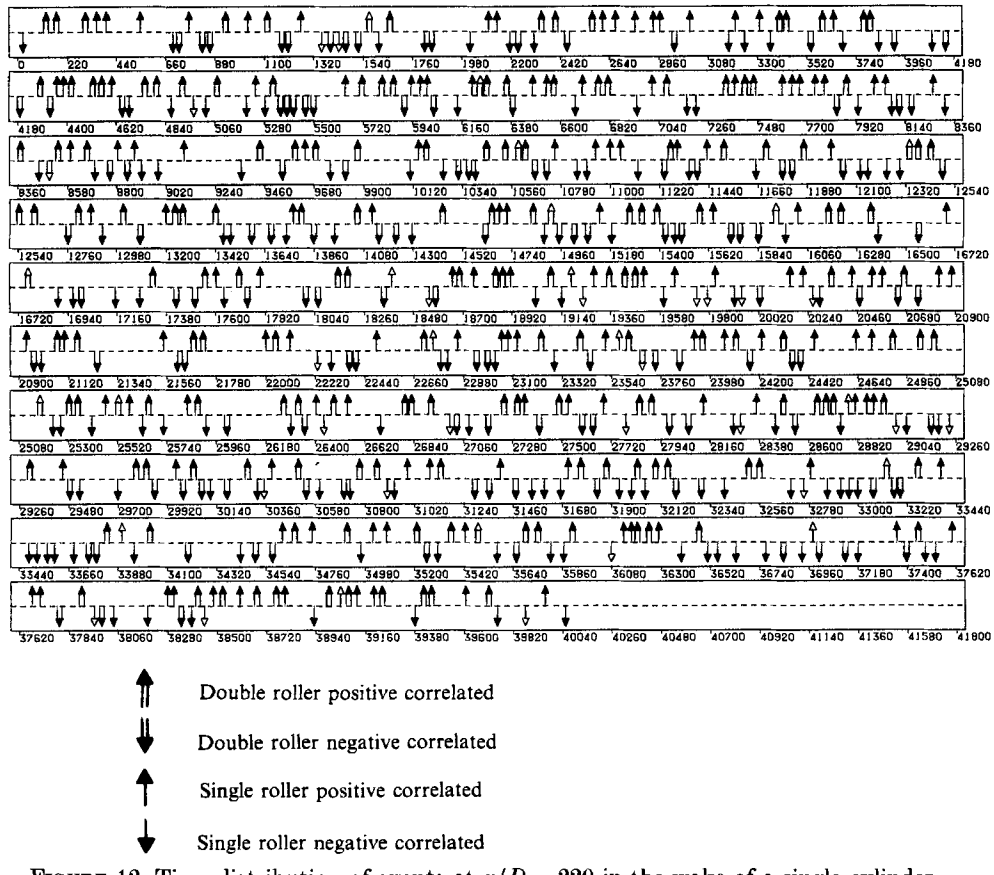

FIGURE 12. Time-distribution of events at $x/D = 220$ in the wake of a single cylinder.

the upper and lower wake, respectively, while the mean velocity profile is quite symmetric. If this difference is taken into account, the peak velocity signals at both sides agree very well. In both cases, the rollers depicted represent about 55% of the flow and the significance level is under 5%.

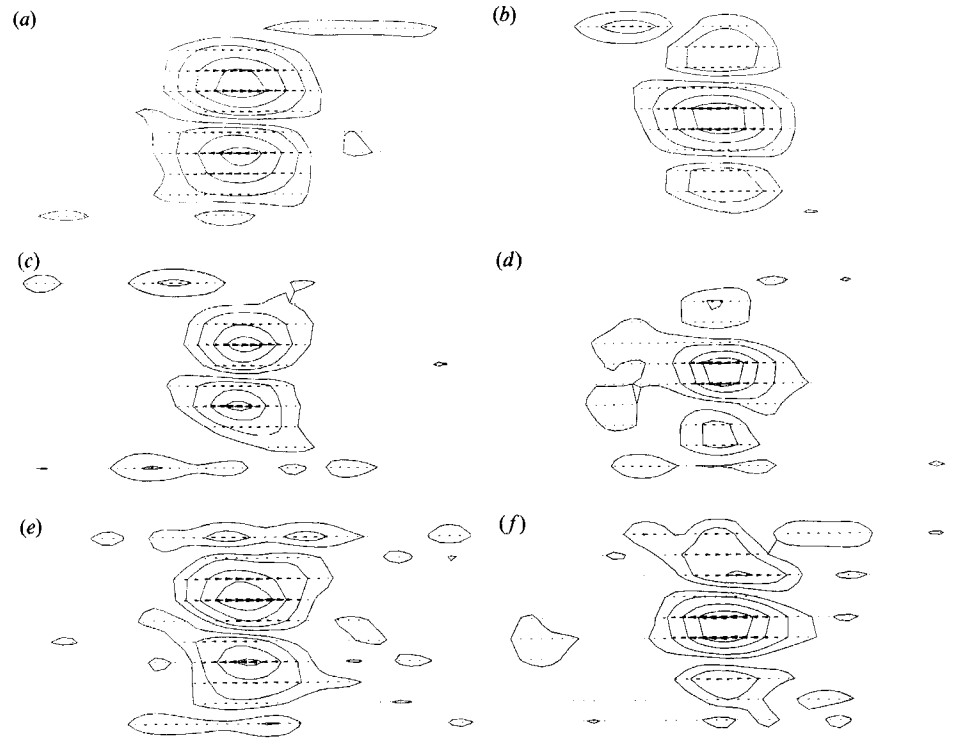

FIGURE 13. Roller eddies at $x/D = 140$. (*a*), (*b*) Cylinder with trailing splitter plate. (*c*), (*d*) Upper side of the wake of a rotating cylinder at $U_p/U_0 = 2$. (*e*), (*f*) Lower side of the wake of a rotating cylinder at $U_p/U_0 = 2$.

Two configurations have been tested in the (z, t)-plane of wakes behind arrays of cylinders, the wake of two unequal diameter cylinders and the wake of a pair of cylinders, one of which is rotating. These two configurations affect the formation of the Kármán vortex street. The first wake is asymmetric owing to the different size of the cylinders, while the second one is forced to become progressively asymmetrical and highly distorted by the rotation of one cylinder from $U_p/U_0 = 0$ to ± 2. In the latter only results for $U_p/U_0 = 0$, i.e. the symmetrical wake, will be presented. The ensemble averages obtained in the upper and lower part of the wake of two unequal diameter cylinder are shown in figure 14 (*a–d*). The peak velocity values are in the range 1.2–1.3 r.m.s. units and the fraction of flow classified is approximately 50%. The rollers detected in the double-cylinder symmetrical wake (figure 14*e*, *f*) are hardly distinguishable from the previous ones. They have peak signal values of 1.35 and the fraction of flow classified is 42%. A common characteristic of all the rollers presented in figure 14 is that they display more scatter than those depicted in figures 10 and 13 for the other wakes studied. This is due to the fact that for a fixed timelength of experiments, if the scales of the flow increase then less flow is recorded and, thus, these ensemble averages were obtained from fewer data frames. In addition, low significance levels are obtained for the 10% contour, ranging from 14% to 20%, and only at the 25% contour is the significance under 1%. Apart from this aspect, the topological features agree extremely well with those of the rollers detected in all the preceding wakes studied.

Common to virtually all the single-roller ensemble averages obtained with the

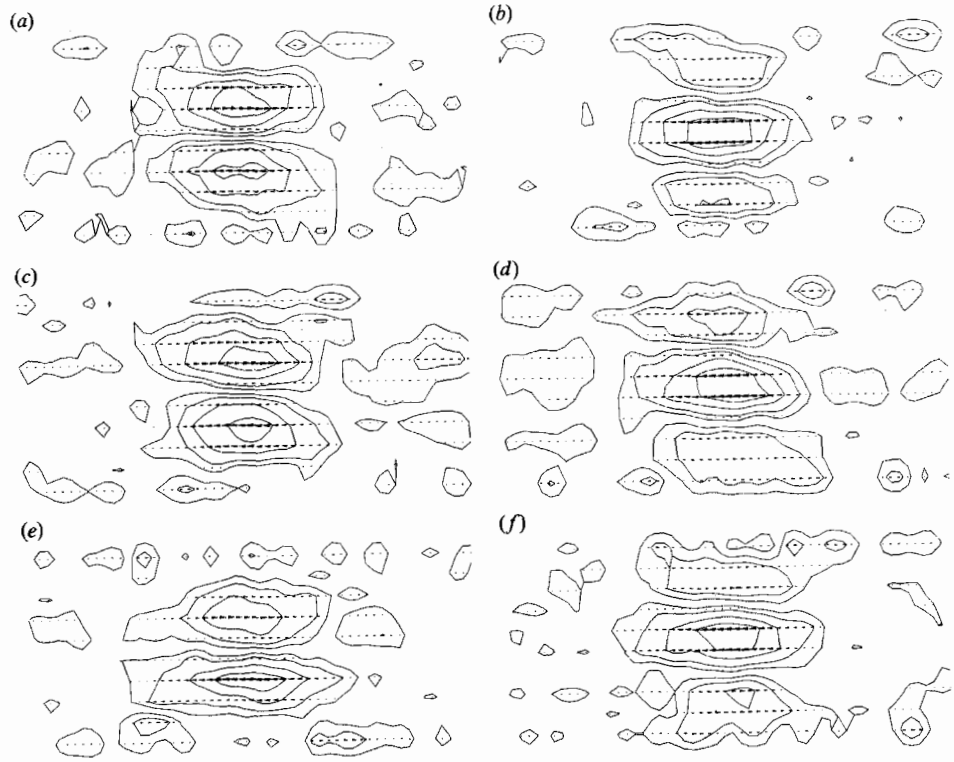

FIGURE 14. Roller eddies at $x/D = 140$. (*a*), (*b*) Upper side of the wake of two unequal cylinders. (*c*), (*d*) Lower side of the wake of two unequal cylinders. (*e*), (*f*) Wake of two equal cylinders.

double-classification algorithm and which are presented in figures 10, 13 and 14 is that they possess additional sign-inverted peak velocities, bounding the velocity lobes corresponding to the single-roller footprint. The only way to explain this result is to accept that the genuine $\omega_{x,y}$ organization in wakes is the double roller. As a consequence, the single rollers detected should be attributed to misalignment of some of the probably larger double rollers present in the flow. In fact, if the analysis is repeated looking for these structures only, more flow is classified because the selection criteria is not so restrictive, the scatter sometimes observable is reduced and the levels of significance are improved. Thus, the uncertainty in deciding between single and double rollers pointed out by Mumford (1983) in his analysis of the wake of a single cylinder, should be solved in favour of the double-roller eddies, in accordance with the early suggestions made by Grant (1958).

The importance of this first conclusion just drawn is to be aware of the displayed similitude of all the rollers detected in the family of wakes studied. Moreover, the size of the rollers (which depends on the half width of the wake), the peak velocities and iso-level contours (which in turn depend on the r.m.s. values) and the fraction of flow they represent (which depends on the generating mechanism and the role played by the rollers in the turbulent budget), range for all the wakes in a narrow band. This fact, together with the different initial conditions of the wakes, as well as the different turbulence intensity levels of the sampling stations, indicates that the double-roller organization could be an intrinsic characteristic of fully turbulent plane wakes. This evidence is highlighted if one takes into account that among the wakes analysed, one

can recognize wakes without initial Kármán vortices or wakes formed merging two single wakes, in addition to the single cylinder wake. If the results obtained by Mumford (1982) in a jet are also considered, it appears that the roller organization could also be a structural characteristic shared by turbulent plane wakes and jets.

The double rollers can be thought to be responsible for the self-preserving behaviour of the wake and for the entrainment process by engulfing, because they scale with the half width of the wake, which properly represents mean wake growth. Furthermore, the unchanging strength of the double rollers when scaled by the r.m.s. values, indicates that the roller-organized motions contain, approximately, the same fraction of the turbulent activity of the wake at any downstream position. Thus, they should be in dynamical equilibrium with the turbulent activity. This equilibrium has to be understood in a strictly dynamical sense; rollers are created, grow, evolve and decay in a continuous way, but the number of double rollers active in the wake remains constant, irrespective of the streamwise coordinate or of the kind of wake, as demonstrated by the fact that the fraction of flow involved in all ensemble averages only varies from 40% to 60%.

Also, the scaling of the rollers with the mean flow parameters and turbulence intensities, suggests that they have to be the active agent maintaining the correlation between u and v velocities, because this is the only significant turbulent quantity that appears in the momentum equation for mean velocities in far wakes. However, circulation in the (x,z)-plane cannot justify the maintenance of this correlation and, thus the circulation axis of the double rollers are expected to be tilted with respect to the vertical axis in the shearwise direction, to take advantage of the stretching produced by the mean strain rate over the shear aligned vortex motions (Tennekes & Lumley 1972). Mumford (1982, 1983) has provided evidence of shear alignment, both in the plane wake and jet. However, the velocity data obtained in the vertical plane of the wake has not been analysed in that sense during the present work, because shear alignment is easily detected in the analysis of a thermally contaminated wake (Ferré & Giralt 1989).

8. The Kármán vortex street and the ω_z-organized motions in far wakes

Facing the similarities exhibited by the different wakes analysed in preceding sections, it is necessary to investigate the role played by the Kármán vortices in the wake development and why large-scale motions in far wakes seem to be insensitive to the initial conditions. Attention will not be focused on the details of the Kármán vortex shedding process, but upon the evolution of the Kármán vortices from the nearest stations, $x/D = 10$, to $x/D = 60$ where they lose their periodic activity (Budny, Kawall & Keffer 1979), as well as to the possibility of survival or regeneration of ω_z-vortices or Kármán-like vortices farther downstream. Therefore, from now on, the analysis will be performed in the u-velocities obtained in a vertical (y,t)-plane, i.e. presenting a side view of the wake (see figure 3 for reference).

Data was obtained in the wake of a single cylinder at $x/D = 10$, 30, 60 and 140, and only at $x/D = 140$ for all the other wakes studied. The anemometers have been placed at $z = 0$ spanning the full velocity defect. At $x/D = 10$ and 30 the mean velocity profile is very far from self-similarity and the anemometer spacing was chosen to be $0.9\,l_0$ instead of $0.6\,l_0$ in order to cover the wake appropriately. In addition, since at $x/D = 10$ no significant randomness in the transverse position of the Kármán vortices was expected, the anemometers were placed covering only from the centre-wake to the outer edge, halving the gap between them. This resulted in

spacing anemometers $0.45\,l_0$ at $x/D = 10$ (covering only half the wake) and $0.9\,l_0$ at $x/D = 30$. For symmetrical wakes at $x/D \geqslant 60$ the anemometers were placed at positions $y = (2.7 - 0.6i)\,l_0$, $i = 1, 2, \ldots, 8$, while for asymmetrical ones the anemometers were centred at the location of the maximum velocity defect maintaining the above mentioned spacing.

8.1. *Evolution of the Kármán vortex street*

Figure 15 shows the velocity signals recorded at $x/D = 10$. Anemometer 8 is in the wake centre-line, while anemometer 1 is in the potential flow. The velocity signals have been scaled by a pooled r.m.s. value to maintain appropriately the relative magnitude of the signals. Simultaneous and periodic fluctuations are apparent in figure 15. It is worth noting the high turbulent content of the signal that, together with the periodicities, shows a broadband spectra extending to the highest frequencies (Gavaldà 1982). Furthermore, it has to be observed that the fluctuations maintain the same sign all across the half wake, while positive and negative fluctuations have different relative magnitudes depending on the position within the wake.

Figure 16(*a*) displays the ensemble-averaged u-velocity footprints of the Kármán vortices at $x/D = 10$. This result corresponds to data recorded in the upper half wake and which were analysed for positive and negative u-fluctuations separately. The two individual plots obtained for positive and negative fluctuations are presented as the upper and lower iso-velocity contours in figure 16(*a*). In both cases the initial test pattern used was 8 anemometers wide, covering only half a vortex, i.e. with only one velocity lobe similar to A or B in figure 16(*a*). Transverse alignment was not allowed because at $x/D = 10$ the Kármán vortices fill the wake and any randomness in the transverse position should be smaller than the sampling grid.

The additional sign-inverted lobes C and D (or E and F), which appear in figure 16(*a*), are the result of the ensemble averaging procedure. They correspond to the Kármán vortices travelling quasi-periodically before and after the vortex triggering the reference signal. The spacing between vortices (C–D distance) matches the experimental Strouhal value of 0.21. The ensemble-averaged Kármán vortices presented in figure 16(*a*) have to be interpreted with caution, mainly when compared with other plots of the near Kármán vortex street (Cantwell & Coles 1983; Kiya & Matsumara 1985). The results presented here do not allow the calculation of stream functions nor of vorticities because they only include u-velocities.

Negative velocity fluctuations contributing to C and D in figure 16(*a*) are the same as those over which B is obtained (the same reasoning can be applied to E, F and A). What is then the cause of the relative weakness of C and D when compared with A, or of E and F when compared with B? The answer is that the pattern-recognition algorithms select individual velocity fluctuations in a window narrower than the displayed one. With this arrangement it is possible to educe any additional organization bounding the prospected structure. The different strength of C or D and A is a consequence of the phase modulation of the Kármán vortex shedding process (Wlezien & Way 1979; Keffer & Kawall 1980), that produces weaker averages in the leading and trailing vortices due to loss of alignment. Usually, the inability of a large-scale detection scheme or of an ensemble averaging procedure to avoid the smearing effects of the phase jitter has been considered a drawback. But in this case it is of fundamental interest to localize the Kármán vortices one by one, so that the frequency history of the vortex street can be determined.

The analysis of the Kármán vortex activity was also carried out at $x/D = 30$ and

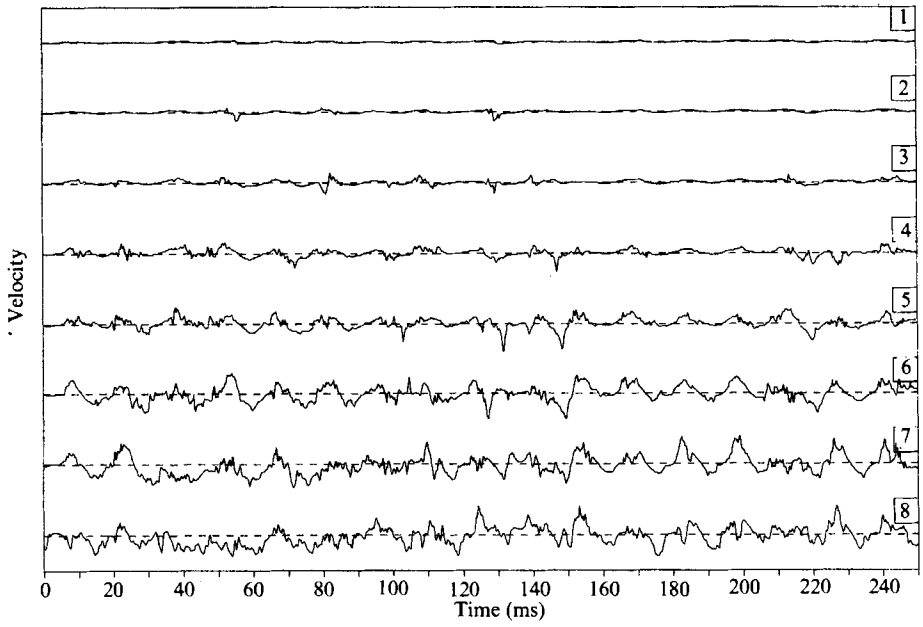

FIGURE 15. Velocity signals at $x/D = 10$ in the upper half wake of a single cylinder.

60, as shown in figure 16(*b*, *c*). A test pattern wider than the velocity signals (12 anemometers in front of 8) was used to allow a more effective search for the structures which should be more randomly distributed in the lateral coordinate. The fact that these or other structures are displayed centred in these and following figures does not mean that they are actually centred in the wake, but that transverse alignment has been allowed. At $x/D = 30$ periodicity is the cause of the additional, weak, velocity contours, which are observed in figure 16(*b*). At $x/D = 60$ no periodicity is evident in figure 16(*c*), although the topology of the averaged vortex is very similar to those depicted at $x/D = 10$ and 30. A comparison of sizes has to take into account that spacing between anemometers was $0.45\,l_0$, $0.9\,l_0$ and $0.6\,l_0$, at $x/D = 10$, 30 and 60, respectively.

What is illustrative is the different values of the peak velocity signal and the number of vortices detected when compared with those shed nominally by the cylinder. Peak velocity values are 2.56, 1.85 and 1.30 r.m.s. units at $x/D = 10$, 30 and 60, respectively, while the fraction of Kármán vortices detected is 63% at $x/D = 10$ and 28% at $x/D = 30$. At $x/D = 60$ the number of structures is still lower, only 22%.

Figure 17 shows the frequency distribution of the Kármán vortices detected at $x/D = 10$, 30 and 60. Even though the histogram is plotted with bars 5 Hz wide, the computed values retain the sampling resolution of 5 kHz. At $x/D = 10$ three zones appear in the histogram. The most populated corresponds to the nominal shedding frequency of 70 Hz. However it broadly ranges from 50 Hz to 85 Hz. A second zone peaks at half the nominal value, while the third one groups the third and lower subharmonics from 10 Hz to 25 Hz. The subharmonics that appear in the histogram are produced by missing cycles of the velocity signals, corresponding to vortices that are very weak or that have been destroyed. For example, in figure 15, between 205 and 220 ms, anemometers 6, 7 and 8 show only random fluctuations where it was expected to observe a new cycle of the Kármán periodic activity. Moreover, the peak

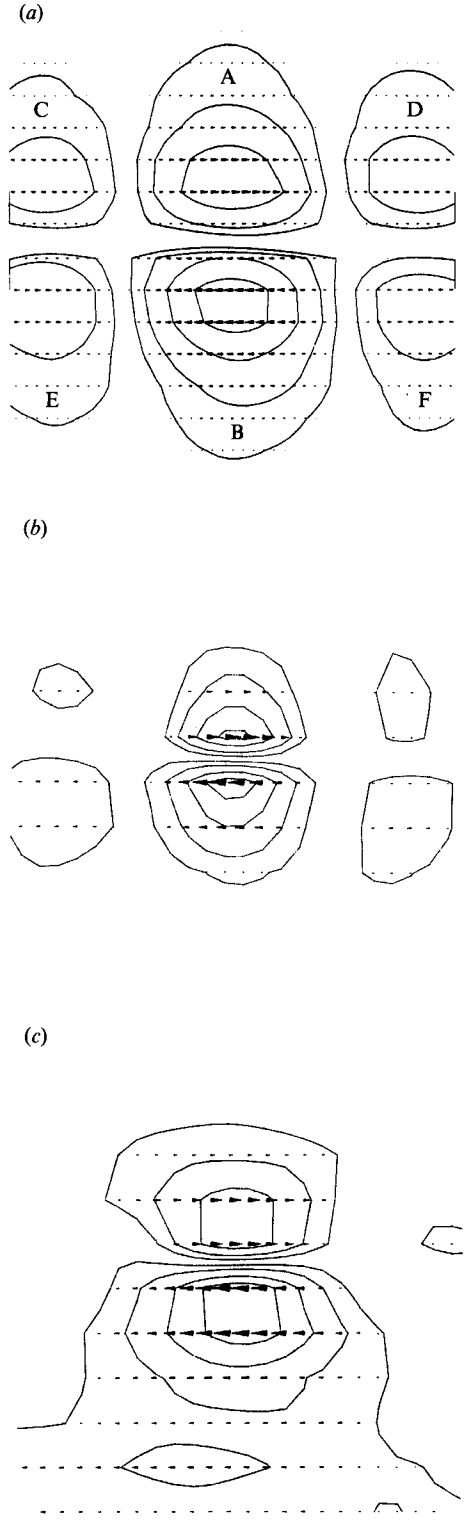

FIGURE 16. Kármán vortices in the wake of a single cylinder. (*a*) $x/D = 10$. (*b*) $x/D = 30$. (*c*) $x/D = 60$.

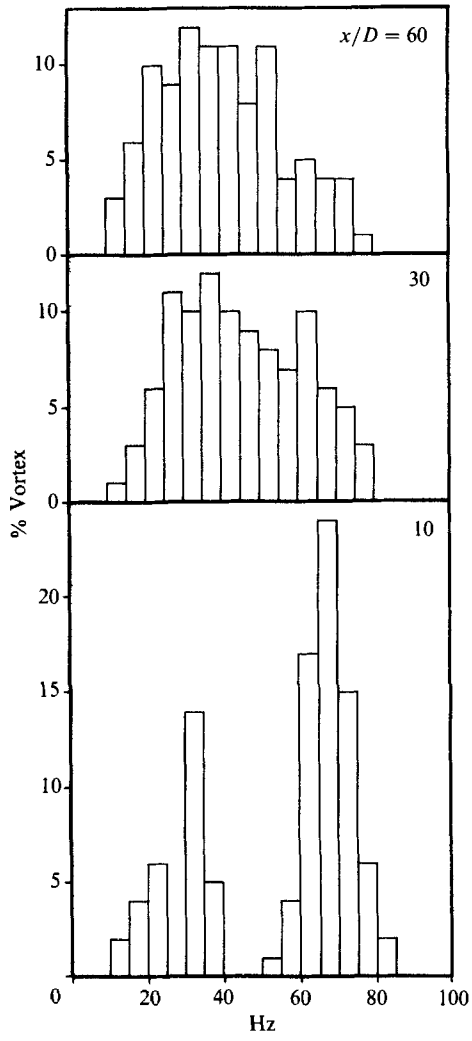

FIGURE 17. Frequency distribution of the Kármán vortices at $x/D = 10$, 30 and 60.

at the nominal frequency is broadband, signalling an early randomization of the vortices within the wake.

The short time-life of the missing vortices at $x/D = 10$, suggests that their destruction should be attributed to disturbances or secondary instabilities rather than to a pure dissipative process. Approximately the same number of vortices are lost between $x/D = 10$ and 30, where only 28% of them are detected. Farther downstream the drop in the number of vortices is not so steep, 22% are detected at $x/D = 60$. This probably corresponds to a change in the mechanism responsible for the decaying process, the dissipative effects playing a more relevant role.

Figure 17 also shows that at $x/D = 30$ the histogram can be interpreted in similar terms. The only difference is that the three previously separated zones overlap, producing a broad frequency distribution from 10 Hz to 80 Hz, with peaks at 35–40 Hz and 60–65 Hz, approximately the first subharmonic and nominal values, respectively. Randomization is total at $x/D = 60$, where a quasi-uniform distribution

from 10 Hz to 60 Hz appears, accompanied by a weak high-frequency zone that perhaps reminds us of the Kármán vortex shedding frequency.

The structural similarities observed between all the ω_z-vortices detected from $x/D = 10$ to $x/D = 60$ and the residual periodic character displayed by the histogram at 60 diameters suggest that the structures detected at this station are also Kármán vortices. In fact individual vortices shed by the cylinder could survive beyond this point. Between $x/D = 30$ and $x/D = 60$ the number of ω_z-vortices detected decreases only from 28% to 22% and the peak velocity from 1.85 to 1.3. These differences indicate that at the latter station Kármán vortices do exist, but with a highly randomized occurrence, as illustrated by the histogram in figure 17. This is the reason why, from the point of view of spectral analysis, Budny *et al.* (1979) reported no significant activity for the Kármán street beyond $x/D = 60$. The application of the more powerful pattern-recognition analysis in the present work has provided more detailed information about the decay of ω_z-vortical structures in the near wake. Note that Kármán vortices coexist at $x/D = 60$ with the roller motions depicted in figure 10(*a*, *b*). The possible relationship between both types of vortical motion is not yet well understood and will be partially dealt with in the following section.

8.2. *ω_z-vortices in the far wake*

Figure 18(*a*) shows the ω_z-vortices detected at $x/D = 140$ in the wake of a single cylinder, while figure 18(*b*) displays the results corresponding to the wake of a cylinder with trailing splitter plate. Although all the wakes included in figure 2 have been analysed, only these two cases are presented here because they display the two extreme behaviours. In the wake of the cylinder with trailing splitter plate, figure 18(*b*), it is possible to detect z-aligned eddies very similar to those observed at $x/D = 60$ in the normal wake (see figure 16*c*) and different from those depicted in figure 18(*a*) for the same wake at $x/D = 140$. This difference, however, is probably due to the use of the diameter as the scaling factor in the wake of the cylinder with splitter plate, where scales are known to be larger. In both wakes, the existence of large-scale motions with ω_z seems to be compatible with the existence of double-roller eddies.

Further observation of the ω_z-structure reported in figure 18(*a*) for the wake of the single cylinder shows that the vortex does not behave as a typical Kármán one, because the effects of shear are noticeable in the alignment. This shear alignment in the 10% and 25% contours, is a genuine feature of the organized motions of the wake, because the initial pattern used was the symmetrical one shown in figure 11(*a*). Shear alignment had also been observed by Mumford (1983) in the far wake. However he was using a template designed to classify the velocity footprints of the roller eddies.

The above results suggest that the far wake is completely dominated by the shear-aligned structures, thus with vorticity in the (x, y)-plane. The fact that the so-called Kármán-like vortex in figure 18(*a*) has both characteristics of ω_z and $\omega_{x,y}$ motions suggests that the features displayed are the combined results of capturing some residual true Kármán vortices, some double-roller effects and also ω_z-motions resulting from the three-dimensional character of the double rollers. Townsend (1979) detected very typical groups of ω_z-eddies at $x/D = 170$ in the wake of a single cylinder. Savill (1979) considered that the double-roller eddies were more than just two counter-rotating eddies, but part of a big horseshoe structure. This structure should have a top linking both rollers, which would contain vorticity aligned with the cylinder axis. These 'tops of the rollers' could be the ω_z-eddies detected by Townsend

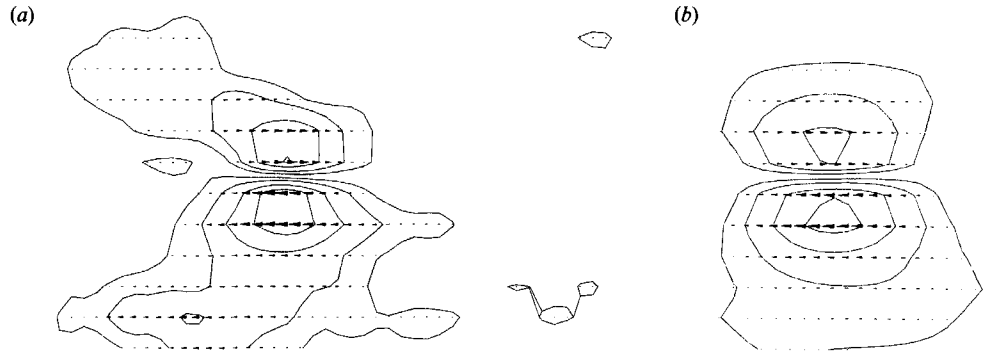

FIGURE 18. ω_z-vortices at $x/D = 140$. (*a*) Single cylinder. (*b*) Cylinder with trailing splitter plate.

(1979) and part of those contributing to the ensemble average of figure 18(*a*). They could also be part of the 'regenerated' Kármán vortex street claimed to have been observed in some visualizations. Nevertheless, it may be concluded that double-roller eddies are the more important large-scale motions in the wake.

9. Concluding remarks

The pattern-recognition computer codes developed in the present work allow the detection, identification and classification of the organized motions present in turbulent flows, as well as the determination of their contribution and importance in turbulence activity. The pattern-recognition procedure applied is flow independent because it has been designed to recognize repetitive trends from any type of stochastic signal, extracting feature axis from the multidimensional pattern space. Noise independence and insensitivity with respect to pattern intensity is achieved by measuring similitude in that space by a correlation coefficient.

The pattern-recognition procedure is more powerful than spectral analysis because it is able to yield equivalent results – the histogram of detection frequency – without losing its ability to detect and obtain ensemble averages of organized motions. The main advantage of pattern recognition when compared with conditional sampling is that there is no need to make use of a triggering signal different from the sampling signals. This is important, not only because it simplifies the experimental set-up, but also because it makes the detection criteria independent of both the energy content and the neatness of the reference signal. In fact, the statistically significant ensemble averages obtained in several wakes have peak signal values of the order of one r.m.s. unit, i.e. the pattern recognition approach is able to select individual realizations as weak as a few r.m.s. units. Therefore, the present technique is, for practical purposes, threshold independent because it has been successfully applied to data with a signal-to-noise ratio of about one, an aspect which the VITA technique lacks despite its widespread use in boundary layers.

The pattern recognition analysis of the near wake behind a single cylinder shows that the decay of the Kármán vortex street activity is already noticeable at $x/D = 10$, where more than 30% of the nominal number of vortices shed have lost their identity as such and are missing. This process of fast destruction of individual vortices, combined with the amplification of other initial disturbances or secondary instabilities and with the dissipative effects of turbulence, results in the ran-

domization of the Kármán vortex street. This randomization, which is very clear at $x/D = 30$ and complete at $x/D = 60$, is the reason why in previous studies the Kármán activity has been claimed to cease at approximately 60 diameters. Nevertheless, present results show that at least 20% of the vortices shed by the cylinder survive beyond this position.

At $x/D = 140$ ω_z-vortices are detected in all wakes studied. However, they do not seem to be related to the Kármán vortex street because in some of the wakes examined this street was inhibited. Moreover, these structures appear also to be dominated by shear alignment and, thus, may in part be the result of footprints left by the three-dimensional $\omega_{x,y}$-structures, rather than of genuine ω_z-eddies. Turbulent flow in far wakes appears to be dominated by double-roller eddies with vorticity aligned with mean shear in the (x, y)-plane. These rollers occupy about 50% of the flow, scale appropriately with the size of the wake and contain approximately the same fraction of the u-velocity turbulent activity, for all wakes examined at downstream positions between $x/D = 60$ and $x/D = 220$. Thus, double-roller eddies could be a large-scale organization typical of self-similar plane turbulent flows.

Financial assistance received from the CICYT and the CIRIT (Generalitat de Catalunya) is acknowledged.

REFERENCES

ALTMANN, J. & REITBROK, H. J. P. 1984 *IEEE Trans. Pattern Analysis Machine Intelligence* **6**, 46–57.

ANDREOPOULOS, J. 1985 *J. Fluid Mech.* **157**, 163–197.

ANTONIA, R. A. 1981 *Ann. Rev. Fluid Mech.* **13**, 131–156.

APELT, C. J. & WEST, G. S. 1975 *J. Fluid Mech.* **71**, 145–160.

BARSOUM, M. L., KAWALL, J. G. & KEFFER, J. F. 1978 *Phys. Fluids* **21**, 157–161.

BLACKWELDER, R. F. 1977 *Phys. Fluids* **20**, S232–S242.

BLACKWELDER, R. F. & KAPLAN, R. E. 1976 *J. Fluid Mech.* **76**, 89–112.

BOW, S.-T. 1984 *Pattern Recognition*. Marcel Dekker.

BROWN, G. L. & ROSHKO, A. 1974 *J. Fluid Mech.* **64**, 775–816.

BUDNY, R. S., KAWALL, J. G. & KEFFER, J. F. 1979 *Proc. Second Intl Symp. on Turb. Shear Flows, London.*

CANTWELL, B. 1981 *Ann. Rev. Fluid Mech.* **13**, 457–515.

CANTWELL, B. & COLES, D. 1983 *J. Fluid Mech.* **136**, 321–374.

CHEN, C-H. P. & BLACKWELDER, R. F. 1978 *J. Fluid Mech.* **89**, 1–31.

CIMBALA, J. M. 1985 *Proc. Fifth Intl Symp. on Turb. Shear Flows, Cornell University.*

CORINO, E. R. & BRODKEY, R. S. 1969 *J. Fluid Mech.* **37**, 1–30.

DAVIES, M. E. 1976 *J. Fluid Mech.* **75**, 209–231.

FABRIS, G. 1979 *J. Fluid Mech.* **94**, 673–709.

FERRÉ, J. A. 1986 Application of an artificial intelligence algorithm to the recognition of coherent structures in turbulent flows (in Catalan). Doctoral thesis, Universitat de Barcelona.

FERRÉ, J. A. & GIRALT, F. 1989 *J. Fluid Mech.* **198**, 65–78.

GAVALDÀ, J. 1982 The wake generated by static and rotating cylinders of equal diameters (in Catalan). Doctoral Thesis, Universitat de Barcelona.

GRANT, H. L. 1958 *J. Fluid Mech.* **4**, 149–190.

HAYAKAWA, M. & HUSSAIN, A. K. M. F. 1985 *Proc. Fifth Intl Symp. on Turb. Shear Flows, Cornell University.*

HUSSAIN, A. K. M. F. 1983 *Phys. Fluids* **26**, 2816–2850.

HUSSAIN, A. K. M. F. 1986 *J. Fluid Mech.* **173**, 303–356.

KEFFER, J. F. 1965 *J. Fluid Mech.* **22**, 135–159.

KEFFER, J. F. 1967 *J. Fluid Mech.* **28**, 183–193.

KEFFER, J. F., KAWALL, J. G., GIRALT, F. & BEGUIER, C. 1982 In *Turbulence in Heat and Mass Transfer*. Hemisphere.

KEFFER, J. F. & KAWALL, J. G. 1980 *AIAA Fluid and Plasma Dyn. Conference, Snowmass, Colorado.*

KIM, H. T., KLINE, S. J. & REYNOLDS, W. C. 1971 *J. Fluid Mech.* **50**, 133–160.

KIYA, M. & MATSUMURA, M. 1985 *Bull. JSME*, **28**, 2617–2624.

LINE, S. J., REYNOLDS, W. C., SCHRAUB, F. A. & RUNSTADLER, P. W. 1967 *J. Fluid Mech.* **30**, 741–773.

KUROSAKA, M. & SUNDARAM, P. 1986 *Phys. Fluids* **29**, 3474–3477.

LAHART, M. J. 1984 *Opt. Engng* **23**, 710–715.

LAUFER, J. 1975 *Ann. Rev. Fluid Mech.* **7**, 307–326.

LU, S. S. & WILLMARTH, W. W. 1973 *J. Fluid Mech.* **60**, 481–511.

LUMLEY, J. L. 1965 *Proc. Intl Colloq. on Atmospheric Turb. and Radio Wave Propagation, Moscow.*

MUMFORD, J. C. 1982 *J. Fluid Mech.* **118**, 241–268.

MUMFORD, J. C. 1983 *J. Fluid Mech.* **137**, 447–456.

PAPAILIOU, D. D. & LYKOUDIS, P. S. 1974 *J. Fluid Mech.* **62**, 11–31.

PAYNE, F. R. & LUMLEY, J. L. 1967 *Phys. Fluids* **10**, S194–S196.

PERRY, A. E. & WATMUFF, J. H. 1981 *J. Fluid Mech.* **103**, 33–51.

PRANDTL, L. & TIETJENS, O. G. 1934 *Applied Hydro- and Aeromechanics.* Dover.

REYNOLDS, W. C. & HUSSAIN, A. K. M. F. 1972 *J. Fluid Mech.* **54**, 263–288.

ROSHKO, A. 1976 *AIAA J.* **14**, 1349–1357.

SAFFMANN, P. G. 1981 In *The Role of Coherent Structures in Turbulence Modelling and Mixing* (ed. J. Jimenez). Lecture Notes in Physics, vol. 136. Springer.

SAVILL, A. M. 1979 Effects on turbulence of curved or distorting mean flow. PhD dissertation, University of Cambridge.

SUBRAMANIAN, C. S., RAJAGOPALAN, S., ANTONIA, R. A. & CHAMBERS, A. J. 1982 *J. Fluid Mech.* **123**, 335–362.

TANEDA, S. 1959 *J. Phys. Soc. Japan* **14**, 843–848.

TENNEKES, H. & LUMLEY, J. L. 1972 *A First Course in Turbulence.* MIT Press.

TOWNSEND, A. A. 1956 *The Structure of Turbulent Shear Flow*, 1st edn. Cambridge University Press.

TOWNSEND, A. A. 1976 *The Structure of Turbulent Shear Flow*, 2nd edn. Cambridge University Press.

TOWNSEND, A. A. 1979 *J. Fluid Mech.* **95**, 515–537.

VAN ATTA, C. W. 1974 *Ann. Rev. Fluid Mech.* **6**, 75–91.

WALLACE, J. M., BRODKEY, R. S. & ECKELMANN, H. 1977 *J. Fluid Mech.* **83**, 673–693.

WALLACE, J. M., ECKELMANN, H. & BRODKEY, R. S. 1972 *J. Fluid Mech.* **54**, 39–48.

WHALEN, A. D. 1971 *Detection of Signals in Noise.* Academic Press.

WLEZIEN, R. W. & WAY, J. L. 1979 *AIAA J.* **17**, 563–570.

YULE, A. J. 1980 In *Turbulent Shear Flows* 2 (ed. L. J. S. Bradbury, F. Durst, B. E. Launder, F. W. Schmidt & J. H. Whitelaw). Springer.

ZILBERMANN, M., WYGNANSKY, I. & KAPLAN, R. E. 1977 *Phys. Fluids* **20**, S258–S271.